JGR Biogeosciences

Key Points:

- Methane clumped isotopologues can fingerprint methane sources, using the Keeling plot method and a new mathematical method
- Methane clumped isotopologue signatures of background air, landfill, and wetland end-members are defined and derived
- Wetland methane emission isotope signals show seasonal variations attributed to microbial oxidation

Constraining Wetland and Landfill Methane Emission Signatures Through Atmospheric Methane Clumped Isotopologue Measurements

Jiayang Sun[1,2,3] (ID)**, Cédric Magen[1]** (ID)**, Mojhgan A. Haghnegahdar[1,4]** (ID)**, Jiarui Liu[5]** (ID)**, Julianne M. Fernandez[1]** (ID)**, and James Farquhar[1,6]** (ID)

[1]Department of Geology, University of Maryland, College Park, MD, USA, [2]Air Resources Laboratory, National Oceanic and Atmospheric Administration, College Park, MD, USA, [3]Cooperative Institute for Satellite Earth System Studies (CISESS), University of Maryland, College Park, MD, USA, [4]Smithsonian Environmental Research Center, Edgewater, MD, USA, [5]Department of Earth, Planetary and Space Sciences, University of California, Los Angeles, CA, USA, [6]Earth System Science Interdisciplinary Center, University of Maryland, College Park, MD, USA

Abstract Microbial methane emissions are associated with a wide range of isotopic signatures, providing information about the sources and sinks of methane. Methods of directly sampling methane from environments such as wetlands may fail to capture the temporal and spatial variations in emissions at a specific site and time. The Keeling plot method is commonly used to infer the overarching isotopic signatures of methane sources. In this study, we have expanded the application of the Keeling plot from conventional stable isotope ratios to include novel clumped isotopologue compositions of methane. This advancement aims to provide more robust constraints on regional methane emission signatures. We analyzed methane isotopologue compositions from air samples collected above wetlands and landfills across Maryland, USA, and determined the end-member compositions for background air, wetland, and landfill sources. Our findings indicate that the isotopologue compositions of methane from regional wetland emissions exhibit seasonal variations—δ^{13}C and δD values become less positive as winter approaches, reflecting changes in methane oxidation and production rates. The continuous monitoring of air methane isotopologue signatures will deepen our understanding of the seasonal patterns in methane emissions and contribute to refining the global methane budget, as valuable insights can be extracted from these measurements.

Plain Language Summary This study extends the method using air measurement to investigate methane emission signatures from wetlands and landfills. Our findings reveal seasonal changes in wetland emission signatures, which are attributed to microbial oxidation.

1. Introduction

Carbon and hydrogen isotopic compositions of methane have proven to be valuable tools for studying microbial methane emissions. Microbial methane refers to methane associated with microbial activities, involving both production and oxidation processes, such as methane from wetlands and landfills. Various factors collectively shape the bulk isotopic signatures of microbial methane emissions, including generation pathways (Hornibrook et al., 1997; Whiticar, 1999; Whiticar et al., 1986), oxidation processes (Alperin et al., 1988; Coleman et al., 1981; Happell et al., 1994), and transport mechanisms (Bastviken et al., 2004; Walter et al., 2008). Analyzing the isotopic signatures of the emitted methane can in turn reveal information about these processes. However, extracting information from bulk carbon and hydrogen isotopes alone could be challenging, as multiple processes could lead to overlapping isotopic characteristics (Liu, Treude, et al., 2023; Milkov & Etiope, 2018).

The measurements of doubly substituted isotopologues (^{13}CH$_3$D and ^{12}CH$_2$D$_2$, hereafter referred to as methane clumped isotopologues) add independent constraints, allowing further exploration of processes related to methane emissions. If the intramolecular isotope exchange of methane reaches thermodynamic equilibrium, the clumped isotopologue signals can be used to constrain the temperatures at which methane formation or equilibration occurs (Stolper, Lawson, et al., 2014; Stolper, Sessions, et al., 2014; Stolper et al., 2015; Young et al., 2017). However, the clumped signals of some natural methane samples deviate from thermodynamic equilibrium (Douglas et al., 2016, 2020; Giunta et al., 2019, 2022; Haghnegahdar et al., 2023, 2024; Liu, Treude, et al., 2023; Wang et al., 2015; Young et al., 2017). Lab-culture experiments and modeling have demonstrated that different

methanogenesis pathways could result in different isotope fractionations of clumped isotopologues (Cao et al., 2019; Giunta et al., 2022; Gropp et al., 2021, 2022; Gruen et al., 2018; Ono et al., 2021, 2022; Rhim & Ono, 2022; Young et al., 2017). Methane oxidation can further cause fractionations (Haghnegahdar, 2018; Krause et al., 2022; Ono et al., 2021; Wang et al., 2016), with oxidation pathways and reversibility scenarios controlling the directions and extents of the fractionation (Giunta et al., 2022; Li, Chiu, et al., 2024; Liu, Harris, et al., 2023).

The diverse control mechanisms on microbial methane emissions pose challenges to using isotopes to investigate these methane sources, which exhibit substantial spatial and temporal variabilities (Burke et al., 1988; Ganesan et al., 2018; Johnson et al., 2022; Walter et al., 2008). For example, even within adjacent areas of the same wetland, or at the same sampling site but sampled at different times, the isotopic signatures of wetland methane can greatly differ. A single sample collected from a lake surface may not indicate whether it represents methane from ebullition or coincidently captures a water turnover event, without additional contextual information (DelSontro et al., 2015; Wik et al., 2016). Point samples can be unrepresentative of overall emissions (DelSontro et al., 2015; Langenegger et al., 2019; Wik et al., 2016).

To overcome biases stemming from high spatial and temporal variability, studies have analyzed isotopes of methane in the air above targeted areas, aiming to provide a more representative snapshot of overall source signatures and their variations (e.g., (Bakkaloglu et al., 2022; Fisher et al., 2011; Sriskantharajah et al., 2012)). This method relies on the assumption that methane emissions from regional upwind sources mix with the atmosphere, with varying degrees of mixing depending mainly on distance. This mixing process is expected to induce linear changes in both methane concentration and its isotopic composition in the downwind air, reflecting the integrated signature of the sources. A common analytical approach to disentangle the mixing of source and background is the Keeling plot method (Bakwin et al., 1998; Keeling, 1958). This technique involves plotting $\delta^{13}C$ and/or δD against the reciprocal of methane concentration ($1/[CH_4]$) in air samples to interpolate the source $\delta^{13}C$ and/or δD values.

Incorporating clumped isotopologues would enhance our capability to differentiate methane sources through atmospheric measurements. Haghnegahdar et al. (2023) reported first measurements of air methane clumped isotopologues and incorporated the results into a global one-box model to delineate the contributions of microbial and thermogenic methane to the global methane budget. A recent study by Haghnegahdar et al. (2024) analyzed air samples collected at various heights from a few centimeters to several meters above the stream and demonstrated that the mixing of wetland methane with air can be traced through clumped isotopologues. Expanding the ideas of Haghnegahdar et al. (2024), this study applied the Keeling plot method to a series of air samples from eastern Maryland to derive the unknown isotopologue signatures of landfills and regional wetlands. The objectives of this study were

1. To explore the variability of methane clumped isotopologue signatures in air influenced by sources, particularly when the air mixes with methane originating from wetlands or/and landfills,
2. To assess the potential of atmospheric methane clumped isotopologues for inferring source compositions in the absence of direct source information, and to determine if the variability in source signatures is reflected in the air measurements, and
3. To conduct atmospheric measurements at a small-scale site to infer methane source signatures, serving as a proof-of-concept to evaluate whether large-scale (e.g., global) atmospheric monitoring of methane clumped isotopologues can effectively provide meaningful insights into source compositions.

2. Samples and Methods

2.1. Sampling Area and Campaigns

The study area is the Patuxent River watershed of the Chesapeake Bay, Maryland, USA. Originating in Maryland's upland area, the Patuxent River flows through the D.C.-Baltimore urbanized corridor before merging into the Chesapeake Bay. This watershed is marked by the presence of abundant natural freshwater tidal wetlands, jousted by agriculture and urbanized areas. Progressing from north to south, there is a gradual increase in salinity levels, influenced by the proximity to the bay and the ocean (Chesapeake Bay Program, 2019, https://www.chesapeakebay.net/what/maps/chesapeake-bay-mean-surface-salinity-1985-2018).
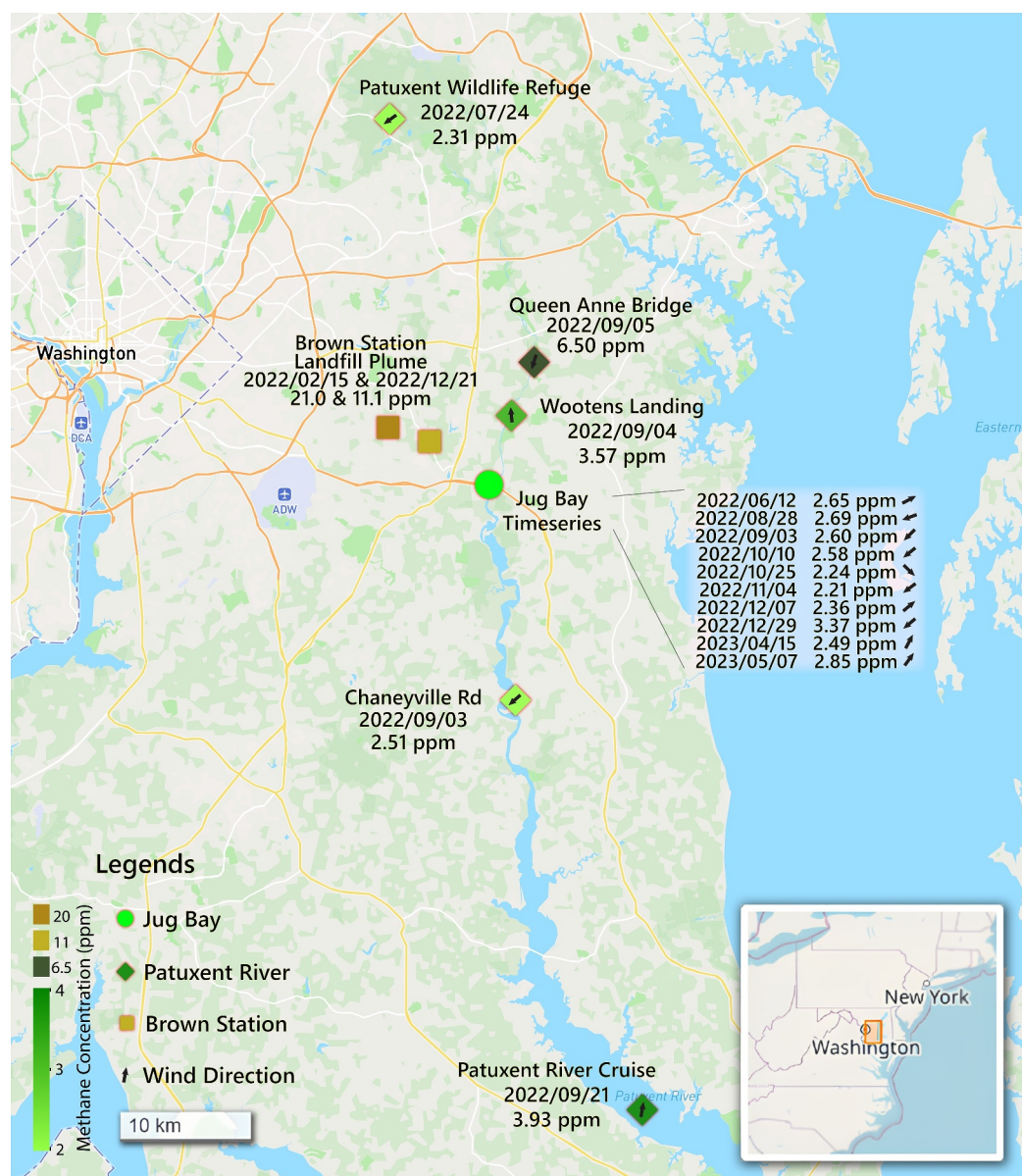
Figure 1. Map of sampling locations. The Jug Bay time series samples are represented by circles with 10 sampling events at the same location. The Patuxent River series samples are shown by diamonds, and landfill air samples by squares. Wetland air samples are in varying shades of green, with darker greens indicating higher methane concentrations. Landfill air is filled with light and dark brown shades. Prevailing wind directions at the time of sampling are indicated by black arrows on the map. The base map was customized using Mapbox. It was then called with the Python Folium package to overlay the base map, add a minimap, and plot data points. Annotations were added in Adobe Illustrator.

Our sampling focused on the Jug Bay Wetlands Sanctuary, with additional samples collected upstream and downstream along the Patuxent River (Figure 1 and Table S1 in Supporting Information S1). The sampling events can be categorized as follows:

1. Time series sampling at the Jug Bay Car Top Boat Launch (hereafter referred to as the Jug Bay), from 12 June 2022, to 7 May 2023. Sampling intervals varied from two weeks to 4 months, with a major pause in sampling activities in early winter 2023.
2. A transect of samples taken along the Patuxent River, from upstream (Patuxent Research Refuge, Bowie, MD) through midstream (Chaneyville Rd, Lower Marlboro, MD) to downstream (Cruise to Patuxent River Station 3), conducted throughout Summer 2023. The Jug Bay is centrally located within this sampling series.

3. Two air samples collected downwind of the Brown Station landfill in Winter 2022 and 2023, during which high methane concentration plumes were detected in mobile greenhouse gas surveys.

Each sampling site is further described in the Supporting Information S1 (Note S1). In the following sections, samples collected above the wetlands from Jug Bay and along the Patuxent River are collectively referred to as "wetland air." Meanwhile, samples that are explicitly influenced by emissions from the Brown Station landfill are referred to as "landfill air."

2.2. Sampling Methods

Sampling was carried out using portable air mattress pumps to inflate Tedlar bags (CEL Scientific Corp.) (Figure S1 and S2 in Supporting Information S1). Approximately 800 L of air were collected for each sample, for a duration of ∼30 min. Sampling dates were picked so that the night before sampling had low wind velocities (<5 mph) to minimize possible horizontal mixing between different local sources. Most samples were collected at or just after sunrise, which provided the greatest likelihood of capturing methane samples before the nocturnal boundary layer dispersed, minimizing the chance of vertical convective mixing that was established during the day. The Patuxent River Cruise sample was collected at noon because it was unsafe for the sampling boat to leave the dock before sunrise. Detailed sampling date, time, and location information can be found in Table S1 in Supporting Information S1.

2.3. Analytical Methods

The samples went through extraction and purification usually on the same day or the next day of sampling. The methodology for these procedures is specifically tailored to fully extracting methane from large volumes of air without causing fractionation (Haghnegahdar et al., 2023). In brief, a cryogenic separation technique is employed to remove substantial quantities of N_2 and O_2 while retaining CH_4 and Kr. A liquid nitrogen-cooled glass condenser was added before introducing the sample into the extraction line for humid samples (Sun, Haghnegahdar, et al., 2025). The preliminarily concentrated gas is then subjected to further separation via gas chromatography (GC) to separate pure methane from other gases. Methane concentrations in each Tedlar Bag were measured using the Aeris MIRA Ultra Methane/Ethane Analyzer (Aeris302) or a GC (Shimadzu® GC-8AIF) before extraction.

We measured the abundances of $^{13}CH_4$, $^{12}CH_3D$, $^{13}CH_3D$, and $^{12}CH_2D_2$ isotopologues relative to $^{12}CH_4$, using the Panorama (Nu Instrument) at the University of Maryland (UMD), College Park, Maryland. Panorama is a high-sensitivity high-resolution gas source mass spectrometer with a mass-resolving power that can distinguish between $^{13}CH_3D$, $^{13}CH_5$ (interference), and $^{12}CH_2D_2$. A comprehensive description of the Panorama instrument and the analytical procedures at UMD can be found in Young et al. (2016) and Haghnegahdar et al. (2023). The measured relative abundances are reported in ratio differences as δ notations:

$$\delta^{13}C_{sample-standard} = \frac{\left(^{13}C/^{12}C\right)_{sample}}{\left(^{13}C/^{12}C\right)_{standard}} - 1 \tag{1}$$

$$\delta D_{sample-standard} = \frac{\left(D/H\right)_{sample}}{\left(D/H\right)_{standard}} - 1 \tag{2}$$

$$\delta^{13}CH_3D_{sample-standard} = \frac{\left(^{13}CH_3D/^{12}CH_4\right)_{sample}}{\left(^{13}CH_3D/^{12}CH_4\right)_{standard}} - 1 \tag{3}$$

$$\delta^{12}CH_2D_{2\,sample-standard} = \frac{\left(^{12}CH_2D_2/^{12}CH_4\right)_{sample}}{\left(^{12}CH_2D_2/^{12}CH_4\right)_{standard}} - 1 \tag{4}$$

The reference standards are Vienna Pee Dee Belemnite (V-PDB) for carbon isotopes and Vienna Standard Mean Ocean Water (V-SMOW) for hydrogen isotopes (Coplen, 1994). The standard for clumped isotopologues ($^{13}CH_3D$ and $^{12}CH_2D_2$) is a hypothetical methane, which adopts the carbon isotope composition from V-PDB and the hydrogen isotope composition from V-SMOW, and assumes an intramolecular stochastic distribution— purely random binding of ^{12}C, ^{13}C, H, and D: (Young et al., 2016)

$$X_{^{13}CH_3D,stochastic} = 4 * X_{^{13}C} * X_D * (X_H)^3 \quad (5)$$

$$X_{^{12}CH_2D_2,stochastic} = 6 * X_{^{12}C} * (X_D)^2 * (X_H)^2 \quad (6)$$

$X_{^{13}C}$ and X_D denote the fractions of ^{13}C and ^2H atoms among the total carbon and hydrogen atoms.

We could further calculate the Δ notations to address the deviations of clumped isotopologue abundances from the stochastic (purely random) state (Eiler & Schauble, 2004; Young et al., 2016):

$$\Delta^{13}CH_3D = \frac{1 + \delta^{13}CH_3D}{(1 + \delta^{13}CH_4) * (1 + \delta^{12}CH_3D)} - 1 \quad (7)$$

$$\Delta^{12}CH_2D_2 = \frac{1 + \delta^{12}CH_2D_2}{(1 + \delta^{12}CH_3D)^2} - 1 \quad (8)$$

The equations presented above are approximations that simplify the calculations. The errors introduced by the approximation are negligible compared to the measurement precision (Haghnegahdar et al., 2023; Sun, Haghnegahdar, et al., 2025). The internal uncertainty is related to measurement duration and instrument conditions. Typically, longer measurement time leads to lower uncertainty, but this requires larger sample volume. The 1SD internal uncertainties are reported in Table S1 in Supporting Information S1 for each sample, and are typically on the order of 0.03‰ for $\delta^{13}C$, 0.1‰ for δD, 0.4‰ for $\Delta^{13}CH_3D$, and 1.5‰ for $\Delta^{12}CH_2D_2$, with a few exceptions (Table S1 in Supporting Information S1). The combined uncertainty is more difficult to estimate, but will be larger than the internal uncertainty as it includes a combination of uncertainty from the instrument and from gas handling and standardization.

2.4. Wind and Water Data

The wind speed and direction, water table depth, salinity, and dissolved oxygen concentration data were acquired from nearby monitoring stations operated by the NOAA National Estuarine Research Reserve System (NERRS, 2025). Detailed descriptions can be found in Supporting Information S1 (Note S2). Wind speeds and directions, and water table depths data are summarized in Table S1 in Supporting Information S1. Salinity and dissolved oxygen concentration are plotted in Figures S1 and S2 in Supporting Information S1.

3. Results

3.1. Methane Concentrations

Methane concentrations in wetland air samples spanned from 2.21 to 6.50 ppm (Table S1 in Supporting Information S1). This range suggests varying degrees of source influence mixing with the air, because background air methane concentrations typically do not reach 2.2 ppm according to NOAA Global Monitoring Lab (GML) data (Lan et al., 2025). One sample collected at the Queen Anne Bridge recorded an unusually high methane concentration of 6.50 ppm, the reason for which remains unclear but is unlikely to be contamination from the landfill plume, given the northward wind direction and the isotope data ($\delta^{13}CH_4 = -52.4‰$ and $\delta^{12}CH_3D = -139.0‰$). Methane concentrations in other wetland air samples did not exceed 4 ppm and mostly ranged between 2.3 and 2.7 ppm, which reflected mixing from the wetlands (see discussions in Section 4), albeit a minor contribution from the Brown Station landfill cannot be excluded. Two samples collected downwind of the Brown Station landfill recorded exceedingly higher methane concentrations of 11.1 and 21.0 ppm, evidently indicating the landfill plume (Environmental Integrity Project, 2021).
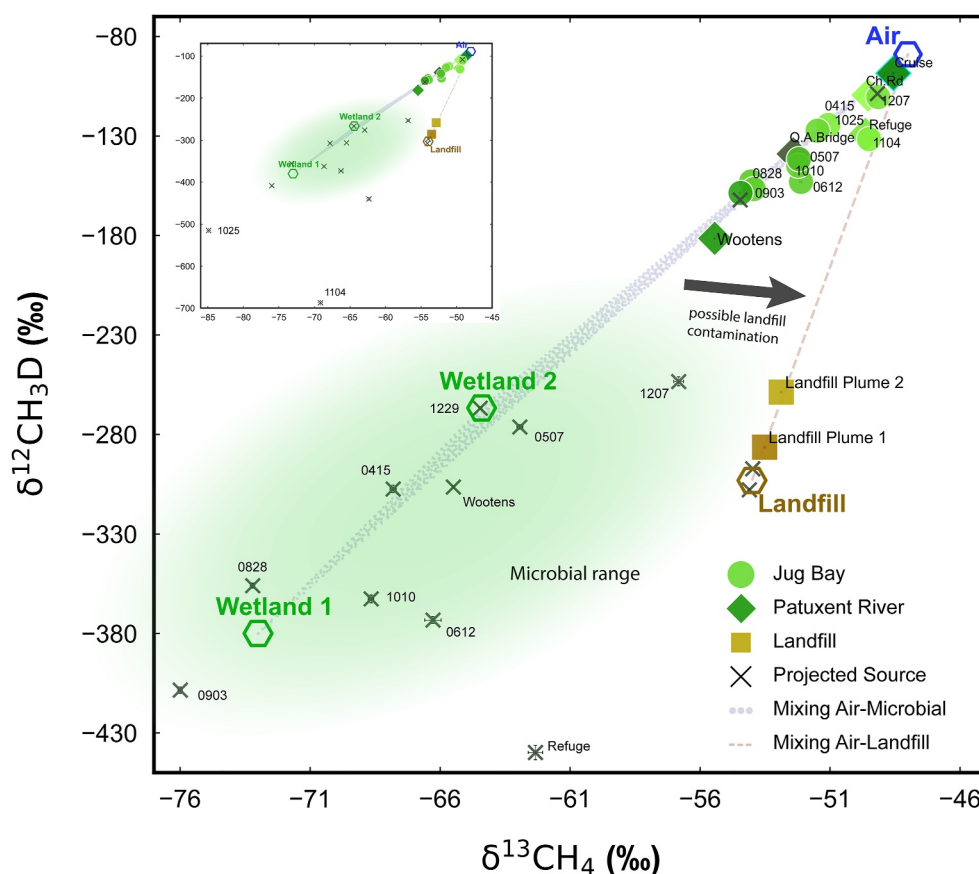
Figure 2. $\delta^{12}CH_3D$-$\delta^{13}CH_4$ plot of samples, together with deduced end-members, projected source compositions, and mixing lines and grids. Hexagonal hollow symbols represent the deduced end-members—blue stands for air, green for wetland, and brown for landfill. The wetland end-member encompasses a broad potential range, approximately shown in transparent green shade. Within this range, "Wetland 1" and "Wetland 2" are two representative compositions. Square solid symbols are two landfill air samples. Diamond-shaped solid symbols represent the Patuxent River series of wetland air samples. Circular solid symbols refer to the Jug Bay time series of wetland air samples. The color gradient of all solid symbols, transitioning from light green to dark green to brown, signifies methane concentrations ranging from near atmospheric levels of 2.2 ppm to the highest 20 ppm. Cross-symbols are the projected source composition calculated based on the end-member values and individual sample values. The small window extends the range of $\delta^{13}C$ and δD to additionally display two calculated values with very depleted compositions. Although these values may exceed the typical isotopic range for natural microbial methane (Liu, 2024), they remain possible (Li, Ash, et al., 2024; Luxem Katja et al., 2020). 1 Standard Deviation (SD) errors for each measurement are plotted on the figure but are smaller than the size of the symbols. Light brown dashed line is the mixing trend of air with landfill end-members. Light gray dots present a mixing grid of air and two microbial end-members.

3.2. Carbon and Hydrogen Isotopes

The isotopic values of wetland air exhibit a wide range, extending from $-48.6‰$ to $-55.4‰$ for $\delta^{13}CH_4$, and from $-98.4‰$ to $-181.4‰$ for $\delta^{12}CH_3D$ (Table S1 in Supporting Information S1 and Figure 2). While the $\delta^{13}CH_4$ values of landfill air fall within the same range as those of wetland air, the $\delta^{12}CH_3D$ values of landfill air are notably more negative, recorded at $-258.7‰$ and $-286.4‰$. Mixing trends for both wetland and landfill are apparent in the $\delta^{12}CH_3D$-$\delta^{13}CH_4$ plot (Figure 2), where a higher proportion of source mixing correlates with more negative $\delta^{12}CH_3D$ and $\delta^{13}CH_4$ values. These mixing scenarios are further discussed in Section 4.

3.3. Methane Clumped Isotopologues

Clumped isotopologue data are presented in Table S1 in Supporting Information S1, Figures 3 and 4. For wetland air samples, $\Delta^{13}CH_3D$ values ranged between $+1.6‰$ and $+3.2‰$. The two landfill samples exhibit $\Delta^{13}CH_3D$ values of $-0.8‰$ and $-0.4‰$, which indicates an anticlumping (negative) $\Delta^{13}CH_3D$ signal of the landfill end-member. The variability is more pronounced in $\Delta^{12}CH_2D_2$: wetland air $\Delta^{12}CH_2D_2$ vary from $+41.5‰$ to

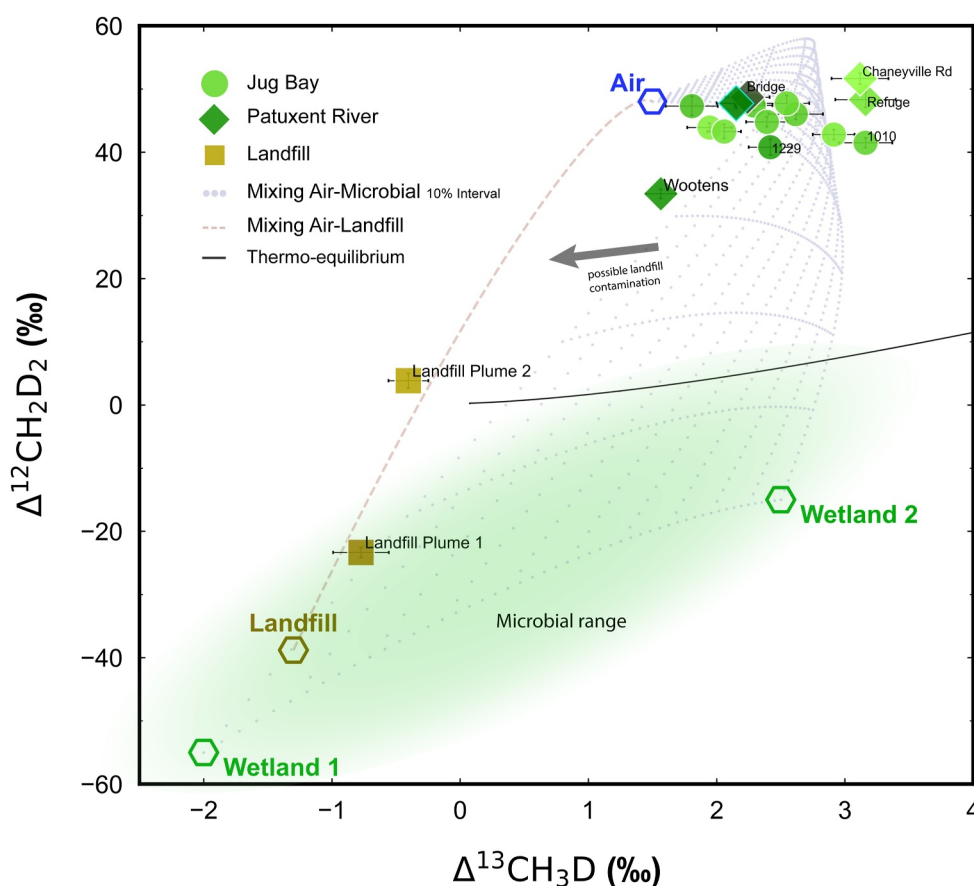**Figure 3.** $\Delta^{12}CH_2D_2$-$\Delta^{13}CH_3D$ plot of samples, together with deduced end-members and mixing lines and grids. The explanation of symbols can be found in Figure 2 caption.

+51.6‰, except for the Queen Anne Bridge sample, which has the highest methane concentration and $\Delta^{12}CH_2D_2 = +33.4$‰. The $\Delta^{12}CH_2D_2$ values of landfill air samples are +3.8‰ and −23.3‰. A greater proportion of wetland and/or landfill mixing leads to more negative $\Delta^{12}CH_2D_2$ values in the mixed air.

4. Discussion

4.1. Mixing

The discussion of mixing is framed within an "Air-Landfill-Wetland three-endmember mixing" framework with five parameters (methane concentration, $\delta^{13}CH_4$, $\delta^{12}CH_3D$, $\Delta^{12}CH_2D_2$, and $\Delta^{13}CH_3D$). The signatures of each end-member remain elusive, as it is usually challenging to acquire representative isotope and isotopologue signatures directly from each source. The mixing scenarios are illustrated in Figures 2–4. The compositions of each end-member are listed in Table 1.

4.1.1. Defining Background Air End-Member Signatures

Defining the concentration and isotopic signatures of background air is the basis for subsequent discussions. Monitoring data from NOAA GML (Lan et al., 2025) and NIST Northeast Corridor (Karion et al., 2020) stations in Washington DC (BWD), Baltimore (NWB and NEB), and northern Maryland (TMD) show that air methane concentrations are not static throughout the year, fluctuating between 1.95 ppm and 2.15 ppm. For our study, we have set 2.05 ppm as the background air methane concentration. Methane concentrations in our study area are elevated slightly above the Northern Hemisphere's tropospheric average because of the Washington D.C.-Baltimore urban plume (Ren et al., 2018) and the inputs from the Marcellus Shale region (Ren et al., 2019).
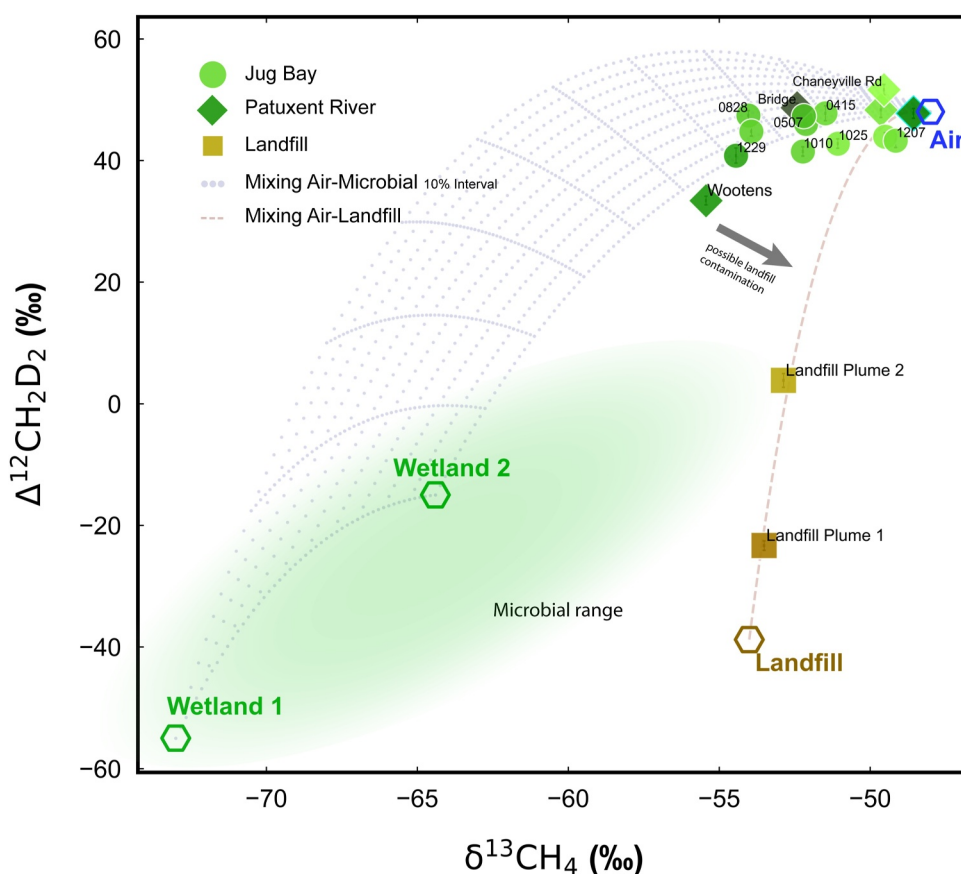
Figure 4. $\Delta^{12}CH_2D_2$-$\delta^{13}CH_4$ plot of samples, together with deduced end-members and mixing lines and grids. The explanation of symbols can be found in Figure 2 caption.

These urban and natural gas field influences are likely also impacting the isotopic compositions of the background air within the study area. Data from the NOAA GML station in Mauna Loa, Hawaii (MLO) show that atmosphere $\delta^{13}C$ values are currently transitioning from $-47.5‰$ to $-48‰$. We can set the lower limit of background air's $\delta^{13}C$ as $-48‰$, assuming that urban air is a mixture of background air and some anthropogenic sources (such as natural gas), which typically have more positive isotopic values.

We conducted isotopologue analysis of "background air" at mid-day over 1 year at the UMD campus. Detailed descriptions of this collection of campus air samples and their compositions are available in Supporting Information S1 (Note S3 and Table S2). The averaged compositions from this set of campus air are $\delta^{13}CH_4 = -47.1‰$, $\delta^{12}CH_3D = -90.2‰$, $\Delta^{13}CH_3D = +1.9‰$, and $\Delta^{12}CH_2D_2 = +46.3‰$, with concentrations between 2.15 and 2.25 ppm. These campus air samples, while informative, may not be pure enough to represent background air at Jug Bay due to potential contamination from local methane sources such as natural gas leakage on the campus. If we consider that UMD air is contaminated by natural gas leakage, $\delta^{13}CH_4 = -47.1‰$ and $\Delta^{13}CH_3D = +1.9‰$ from the averaged UMD campus air can be regarded as the upper limit, while $\delta^{12}CH_3D = -90.2‰$ and $\Delta^{12}CH_2D_2 = +46.3‰$ can be the lower limit of the background air.

In this study, we set methane concentration at 2.05 ppm, $\delta^{13}CH_4$ at $-48.0‰$, $\delta^{12}CH_3D$ at $-89.0‰$, $\Delta^{13}CH_3D$ at $+1.5‰$, and $\Delta^{12}CH_2D_2$ at $+48.0‰$, as regional background air methane compositions (Table 1). We will proceed by treating the air compositions as fixed in our subsequent discussions, which is a simplification that may introduce some errors. Nonetheless, the primary goal of this study is to develop a methodology that incorporates clumped

Table 1
The Compositions of Each End-Member That Are Used in the Discussion

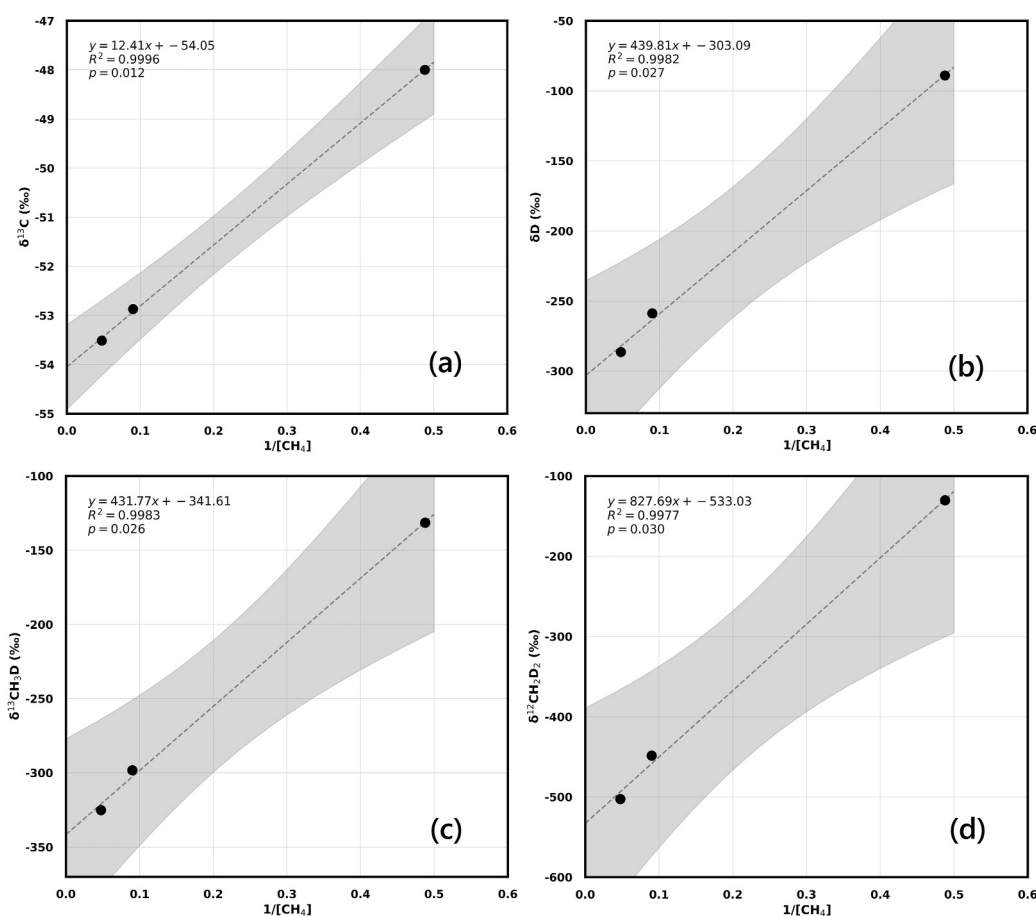| End-member	[CH₄]	$\delta^{13}C$ ‰	δD ‰	$\Delta^{13}CH_3D$ ‰	$\Delta^{12}CH_2D_2$ ‰
Air	2.05 ppm	−48.0	−89.0	1.5	48.0
Landfill		−54.0	−303.1	−1.3	−38.8
Microbial 1		−73.0	−380.0	−2.0	−55.0
Microbial 2		−64.4	−266.7	2.5	−15.0
Microbial		−68.7	−323.4	0.8	−24.9
Natural gas		−37.0	−160.0	2.0	8.0
Total source		−54.2	−295.0	1.5	−20.0

Figure 5. (a) $\delta^{13}CH_4$, (b) $\delta^{12}CH_3D$, (c) $\delta^{13}CH_3D$, and (d) $\delta^{12}CH_2D_2$ three-point Keeling plots for landfill air samples. The point in the upper right corner of each panel is the defined background air, and the two points in the lower left corner are landfill air samples. The gray bands represent the 95% confidence intervals of each linear fit.

isotopologue data to deduce source characteristics from air measurements. Considering the limited precision and availability of data on air methane clumped isotopologue measurements, which restrict our ability to discern minor variations in the background air, this simplification is deemed acceptable.

4.1.2. Determining Landfill Emission Signatures

The isotopologue compositions of the Brown Station landfill end-member during winter were derived from the defined background air compositions and the measured values from landfill air sample values using a three-point Keeling plot approach (Figure 5). It yields $\delta^{13}CH_4 = -54.0‰$, $\delta^{12}CH_3D = -303.1‰$, $\delta^{13}CH_3D = -341.6‰$, and $\delta^{12}CH_2D_2 = -533.0‰$. Subsequently, we can calculate $\Delta^{13}CH_3D = -1.3‰$ and $\Delta^{12}CH_2D_2 = -38.5‰$ using the equations in Section 2.3. Two-point inversions for the 21.0 and 11.1 ppm landfill air samples separately yield similar results. These projected $\delta^{13}CH_4$ and $\delta^{12}CH_3D$ values align with the range provided by onsite landfill measurements (Bakkaloglu et al., 2021). However, because we only sampled the plume outside one landfill, and both two samples were collected during winter, the seasonal and site-specific variabilities of the landfills (Spokas et al., 2021) are not within the scope of this study.

4.1.3. Determining Wetland Emission Signatures

The Keeling plot method was also applied to wetland air samples (Jug Bay and Patuxent River series) (Figure 6). Most samples exhibit a positive linear correlation between $\delta^{13}CH_4$ and $\delta^{12}CH_3D$ with $1/[CH_4]$, yielding a derived wetland methane composition of $\delta^{13}CH_4 = -64.7‰$, $\delta^{12}CH_3D = -273.4‰$, $\delta^{13}CH_3D = -321.2‰$, and $\delta^{12}CH_2D_2 = -480.7‰$. These values fall in the mix and transition zone of two primary methanogenesis pathways

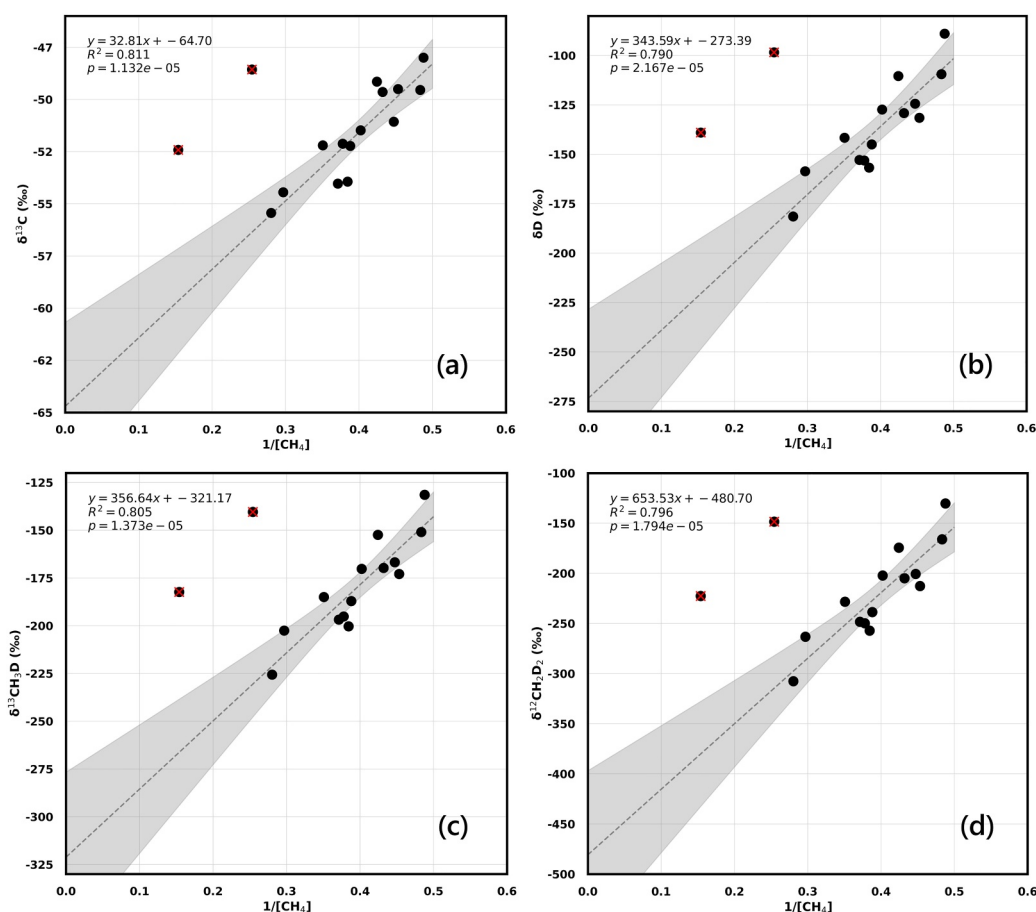**Figure 6.** (a) $\delta^{13}CH_4$, (b) $\delta^{12}CH_3D$, (c) $\delta^{13}CH_3D$, and (d) $\delta^{12}CH_2D_2$ Keeling plots for all wetland air samples. The one point in the upper right corner of each panel is the defined background air, and the rest of the points are wetland air samples. Two outliers (Queen Anne Bridge and the Patuxent River cruise) off the major linear array are each marked with a red cross. The gray bands represent the 95% confidence intervals of each linear fit.

(hydrogenotrophic and acetotrophic) (Conrad, 2005) as categorized by Whiticar (1999). Methanogenic pathways other than CO_2 reduction and acetate fermentation, such as methanogenesis using methanol and methyl amine, cannot be ruled out. However, these pathways are not predominant under natural freshwater wetland conditions, and there is no evidence to suggest substantial activity of such pathways in the study area (Haghnegahdar et al., 2024). We calculated $\Delta^{13}CH_3D = -1.1‰$ and $\Delta^{12}CH_2D_2 = -16.4‰$. The derived $\Delta^{13}CH_3D$ aligns with typical characteristics of wetland methane. The $\Delta^{12}CH_2D_2$ value, while showing less anticlumping than direct field methane samples from wetlands (Haghnegahdar et al., 2024), is consistent with methane produced in lab pure cultures using hydrogen and CO_2 as the substrates (Giunta et al., 2019; Young, 2019). This $\Delta^{12}CH_2D_2$ value may also reflect the influence of either aerobic or anaerobic oxidation in an open system, where the original anticlumping signals are erased as oxidation proceeds (Krause et al., 2022; Liu, Harris, et al., 2023; Ono et al., 2021). Figure 6 also reveals that samples from the Queen Anne Bridge and the Patuxent River cruise deviate from the main linear array, suggesting the possible contribution of diverse methane sources or additional processes affecting the isotopic composition at these specific locations.

However, the application of the Keeling plot across all wetland air samples may be flawed due to the underlying oversimplification that the isotopic compositions of the wetland end-member are constant. To address this issue, we explored by applying the two-point Keeling method to each individual wetland sample, treating each as a unique mixture of the previously determined constant background air and specific methane emissions at the time of sampling. The derived end-member compositions and associated uncertainties are listed in Table S3 in Supporting Information S1, and the $\delta^{13}CH_4$ and $\delta^{12}CH_3D$ values are projected in Figure 2. A notable limitation of this method is the amplification of small measurement uncertainties, particularly when methane concentrations and

isotopic compositions in the sample closely resemble those of the background air. The two-point Keeling plot method seems to be less reliable when projecting clumped isotopologue signals, a frequently yielding unrealistic compositions (Table S3 in Supporting Information S1) due to the disproportionate amplification of biases and uncertainties in concentration, $\delta^{13}CH_4$, $\delta^{12}CH_3D$, $\Delta^{13}CH_3D$, and $\Delta^{12}CH_2D_2$ values during the inversion.

Although the Keeling plot method can yield unreliable results when applied to wetland air samples, particularly for clumped isotopologues, we still selected two sets of nominal values (listed in Table 1 and illustrated in Figures 2–4) to represent the wetland methane isotopic signatures while also reflecting the observed variability. The first set, labeled "Wetland 1," has $\delta^{13}CH_4 = -73.0‰$, $\delta^{12}CH_3D = -380.0‰$, $\Delta^{13}CH_3D = -2.0‰$, and $\Delta^{12}CH_2D_2 = -55.0‰$, referencing studies by Haghnegahdar et al. (2024) and Giunta et al. (2019). We hypothesize that this end-member represents methanogenesis using methyl compounds and acetate as substrates and/or involves low metabolic reversibility during methanogenesis (Giunta et al., 2019; Gropp et al., 2022; Ono et al., 2022). The second set, "Wetland 2," has $\delta^{13}CH_4 = -64.4‰$, $\delta^{12}CH_3D = -266.7‰$, $\Delta^{13}CH_3D = +2.5‰$, and $\Delta^{12}CH_2D_2 = -15.0‰$, cited from Giunta et al. (2022); Haghnegahdar (2018); and Young (2019). This end-member may reflect methanogenesis using hydrogen and CO_2 as substrates and/or high metabolic reversibility during methanogenesis (Giunta et al., 2019; Gropp et al., 2022; Ono et al., 2022). It may also represent microbial methane that has undergone a higher degree of oxidation (Giunta et al., 2022; Liu, Harris, et al., 2023; Ono et al., 2021), thus exhibiting less negative $\delta^{13}C$ and δD, together with a less anticlumping clumped signal. These values were chosen solely for facilitating discussions and visualizations, while covering the majority of the derived wetland end-member compositions (Figures 2–4). This suggests that most samples likely represent different degrees of mixing between air and methane from wetlands, with varying methanogenesis pathways and reversibility, and/or oxidation levels.

4.1.4. Constraining Bulk Isotopic Compositions With Clumped Isotopologues

In Section 4.1.3, we revealed that using measured wetland air compositions to determine source compositions could result in significant uncertainties and yield unreasonable outcomes, especially for clumped isotopologues. These inaccuracies are partly attributed to variability in air composition, where the assigned values may not accurately represent the actual background air compositions at each sampling event. Another source of error stems from inaccuracies in concentration measurements. Our sampling protocol involves collecting over 600 L of air per sample in three or four 200-L Tedlar bags. Filling each bag takes about 15 min, with two bags often being filled simultaneously. We have noted concentration discrepancies between bags as high as 0.2 ppm, exceeding the precision of the Aeris gas analyzer (1 SD = 1.6 ppb with 1-s integration). This suggests that the air above the sampling area might be heterogeneous, or that methane concentrations can fluctuate substantially over sampling periods. These inaccuracies and uncertainties will be amplified during the inversion processes used to calculate projected source compositions.

We can use the derived $\Delta^{13}CH_3D$ and $\Delta^{12}CH_2D_2$ from Section 4.1.3 as a check of the results. These derived $\Delta^{13}CH_3D$ and $\Delta^{12}CH_2D_2$ values were found to be unreasonable for samples: 20220612 Jug Bay, 20220724 Patuxent, 20220828 Jug Bay, 20220903 Jug Bay, 20220903 Patuxent, 20221010 Jug Bay, 20221025Jug Bay, and 20221104 Jug Bay. This underscores the necessity for more precise methane concentration profiles and more stringent constraints on air isotopologue compositions through more collection of background air samples. The checks provided by $\Delta^{13}CH_3D$ and $\Delta^{12}CH_2D_2$ are invaluable for evaluating data quality and the validity of extracted values.

To address the challenges, we explored a novel approach that leverages the additional constraints provided by methane clumped isotopologues (Δ values) to deduce the bulk (carbon and hydrogen) isotopic compositions (δ values) of the source methane, independently of concentration data. This methodology hinges on a critical assumption, supported by existing literature (Giunta et al., 2019, 2022; Haghnegahdar, 2018; Haghnegahdar et al., 2023, 2024; Liu, Harris, et al., 2023; Taenzer et al., 2020; Young, 2019; Young et al., 2017) that the $\Delta^{12}CH_2D_2$ signature of microbial methane typically falls within a certain range. We allow a broad range for $\Delta^{12}CH_2D_2$ between $-5‰$ and $-55‰$ to cover most of the $\Delta^{12}CH_2D_2$ values reported for natural microbial methane. With this defined range, we are able to estimate the wetland's (bulk) hydrogen isotope composition ($\delta^{12}CH_3D_{source}$) using the following parameters: the presumed background air isotope and isotopologue compositions (R_{air}) and the measured isotope and isotopologue compositions of wetland air samples (R_{source}), without concentrations:
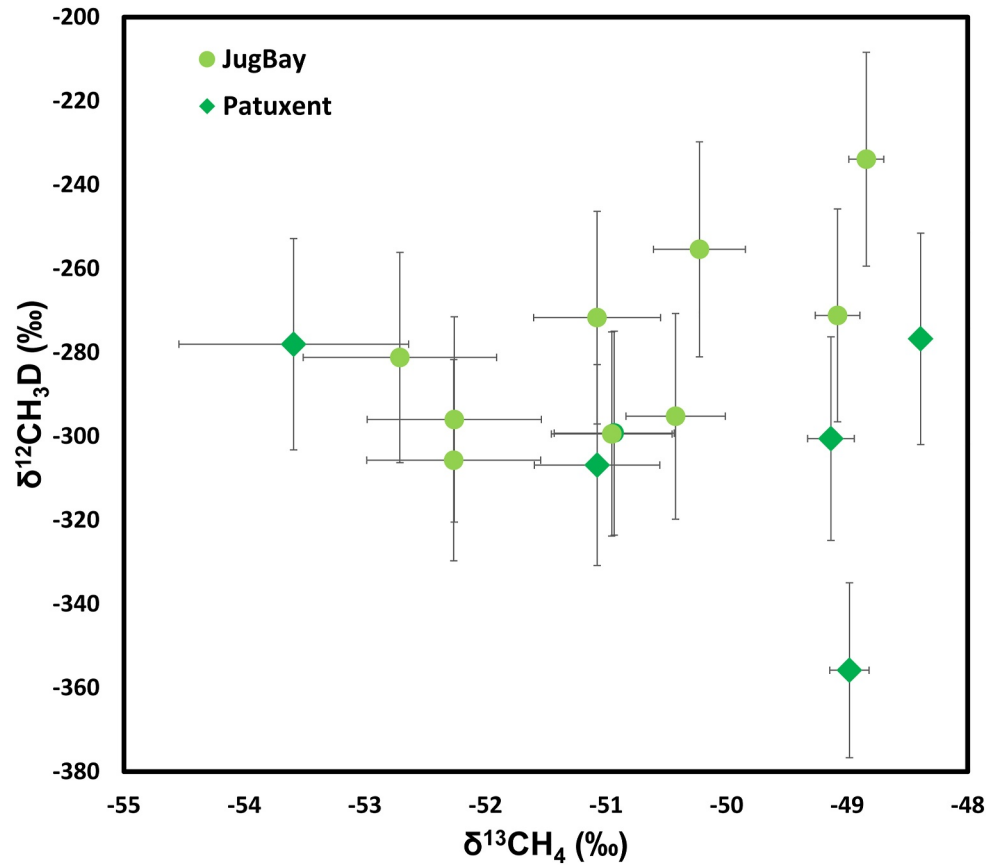
Figure 7. Derived bulk hydrogen and carbon isotope compositions and uncertainties of the source methane ($\delta^{12}CH_3D_{source}$ and $\delta^{13}CH_{4,\,source}$) for each wetland air sample. Source compositions derived from the Jug Bay air samples are in light green circles, and those derived from the Patuxent air samples are in dark green diamonds.

$$\left(1 + \frac{\Delta^{12}CH_2D_{2_{source}}}{1000}\right) * RD_{source}{}^2 - \left(\frac{RD2_{mix} - RD2_{air}}{RD_{mix} - RD_{air}}\right) * RD_{source}$$
$$+ \left(\frac{RD2_{mix} - RD2_{air}}{RD_{mix} - RD_{air}}\right) * RDair - RD2_{air} = 0 \tag{9}$$

R is the normalized ratio of isotopologue abundances. The definitions and mathematical derivations are detailed in Supporting Information S1(Note S4). This equation provides a way to infer $\delta^{12}CH_3D_{source}$ (results listed in Table S5 in Supporting Information S1 and illustrated in Figure 7) by utilizing the constraints imposed by $\Delta^{12}CH_2D_{2\,source}$, hence offering a new perspective on source characterization without the direct need for concentration values. When the $\Delta^{12}CH_2D_2$ value approaches its minimum of −55‰, the calculated δD becomes more negative, with an average around −316‰. Conversely, when $\Delta^{12}CH_2D_2$ nears its maximum of −5‰, the calculated δD is less negative, averaging approximately −268‰. The 50‰ large variation range of $\Delta^{12}CH_2D_2$ propagates to an uncertainty of about 24‰ in δD, which is smaller than the inferred variation range of the methane δD signal in the studied wetland area (approximately 60‰, ranging from −300‰ to −240‰, see Figure 8) and significantly less than the variability of δD signals for natural microbial methane, which spans approximately 250‰ (from around −400‰ to −150‰).

Delving deeper following this idea, we consider that the $\Delta^{13}CH_3D$ and $\Delta^{12}CH_2D_2$ values of microbial methane are governed by a unified process, including changes in methanogenesis pathways and metabolic reversibility, and the involvement of microbial oxidation. We suggest that there exists a mathematical relationship between $\Delta^{13}CH_3D$ and $\Delta^{12}CH_2D_2$, that is, $\Delta^{13}CH_3D_{microbial} = f(\Delta^{12}CH_2D_{2_{microbial}})$, for microbial methane. This hypothesis aligns with experimental and modeling research that seeks to elucidate the behavior of microbial
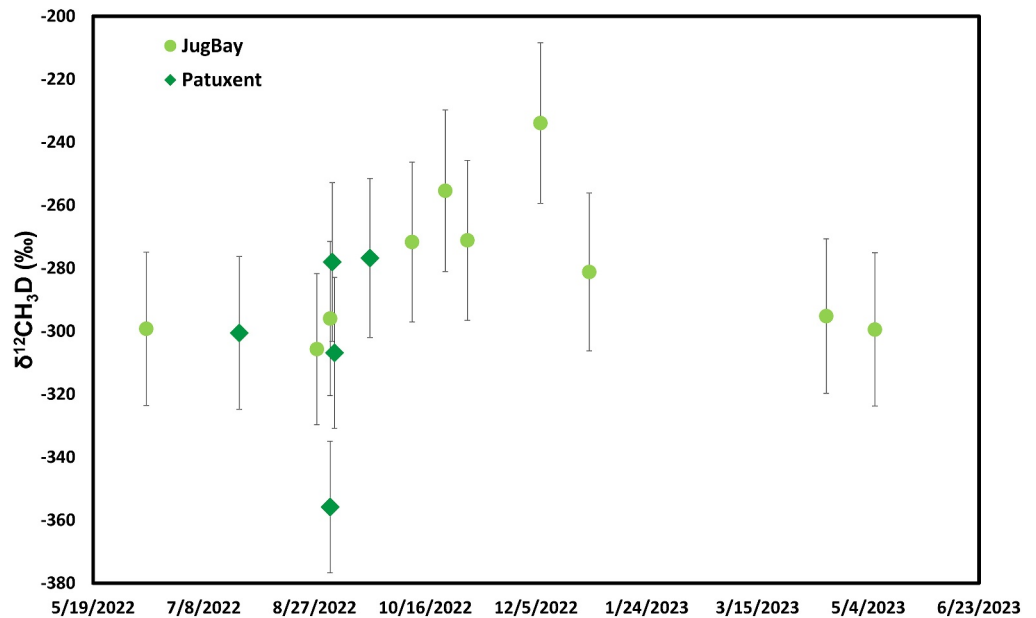
Figure 8. Calculated bulk hydrogen isotopic composition ($\delta^{12}CH_3D_{source}$) versus sampling time. Source compositions derived from the Jug Bay air samples are in light green circles, and those derived from the Patuxent air samples are in dark green diamonds.

methane clumped isotopologues (Cao et al., 2019; Gropp et al., 2021; Liu, Harris, et al., 2023; Ono et al., 2021; Wang et al., 2015). Generally, a more negative $\Delta^{12}CH_2D_2$ is associated with a more negative $\Delta^{13}CH_3D$. Compiling the available natural methane, incubation methane, and lab-culture methanogenesis methane clumped isotopologue data from Giunta et al. (2019, 2022), Haghnegahdar et al. (2023, 2024), Li, Ash, et al. (2024), Liu, Harris, et al. (2023), Young (2019), and Young et al. (2017) (see Note S4, Table S4, and Figure S5 in Supporting Information S1), without accounting for specific physical or biological processes, we establish a simplistic linear relationship between $\Delta^{13}CH_3D$ and $\Delta^{12}CH_2D_2$ values of microbial methane:

$$\Delta^{13}CH_3D_{\text{wetland methane}} = (5.70 \pm 0.26) * \Delta^{12}CH_2D_{2\text{wetland methane}} - (28.99 \pm 0.95) \tag{10}$$

With this established relationship, we can proceed to estimate the source's bulk carbon isotope composition using the designated $\Delta^{12}CH_2D_2$ range as follows:

$$RC_{\text{source}} = \frac{RCD_{\text{air}} - \left(\frac{RCD_{\text{mix}} - RCD_{\text{air}}}{RC_{\text{mix}} - RC_{\text{air}}}\right) * RC_{\text{air}}}{\left(1 + \frac{f\left(\Delta^{12}CH_2D_{2\text{source}}\right)}{1000}\right) * RD_{\text{source}} - \left(\frac{RCD_{\text{mix}} - RCD_{\text{air}}}{RC_{\text{mix}} - RC_{\text{air}}}\right)} \tag{11}$$

The definitions and mathematical derivations are detailed in Supporting Information S1 (Note S4). This equation can be used to infer $\delta^{13}CH_{4,\text{ source}}$ (results listed in Table S5 in Supporting Information S1 and illustrated in Figure 7) based on the assumed range of the $\Delta^{12}CH_2D_{2\text{ source}}$ and the assumed linear relationship between $\Delta^{13}CH_3D_{\text{source}}$ and $\Delta^{12}CH_2D_{2\text{ source}}$. With the 50‰ variation range of $\Delta^{12}CH_2D_2$, the corresponding uncertainty in $\delta^{13}C$, based on the aforementioned assumptions, averages only about 0.8‰. This uncertainty is less than the inferred variation range of the methane $\delta^{13}C$ signal in the studied wetland area (approximately 5.1‰, ranging from −53.5‰ to −48.4‰), and is significantly smaller than the variability of $\delta^{13}C$ signals for natural microbial methane, which spans approximately 40‰ (ranging from around −90‰ to −50‰).

However, the calculations in Section 4.1.4, constrained by clumped isotopologues, derived wetland methane carbon and hydrogen isotopic signatures that are significantly less negative (δD approximately −290‰ and $\delta^{13}C$ approximately −51‰) compared to those calculated through the Keeling plot method in Section 4.1.3 (δD approximately −320‰ and $\delta^{13}C$ approximately −65‰). The signatures from Section 4.1.4 are more similar to

those of the landfill end-member calculated in Section 4.1.2 using the Keeling plot method. While the results from Section 4.1.4 show notably smaller uncertainties and less unreasonable scattering, the method also involves some assumptions. Future work will require more combined air and direct field sampling, along with high-precision concentration and isotopologue measurements, to determine which method yields the most reasonable results.

4.2. The Variability of Isotopic Composition of Wetland Methane Emissions

As mentioned in the introduction, multiple factors can influence the isotopic signatures of wetland methane emissions, including methanogenesis pathways and metabolic reversibility, oxidation processes, and transport mechanisms. Microbial methane can be generated through several different pathways: hydrogenotrophic, acetotrophic, and methylotrophic methanogenesis. Each pathway tends to yield different isotopic signatures (Hornibrook et al., 1997; Whiticar et al., 1986). For example, methane produced through the hydrogenotrophic pathway is generally more depleted in ^{13}C (with $\delta^{13}C$ values typically ranging from $-110‰$ to $-60‰$) and less depleted in D (with δD values usually ranging from $-350‰$ to $-170‰$). In contrast, methane generated through the acetotrophic pathway generally shows $\delta^{13}C$ values ranging from $-70‰$ to $-50‰$ and δD values from $-400‰$ to $-250‰$ (Whiticar, 1999).

Microbial methane oxidation complicates the interpretation of carbon and hydrogen isotopic signatures, as it alters the signals (Alperin et al., 1988; Coleman et al., 1981; Happell et al., 1994). Aerobic oxidation of methane (AeOM) typically results in both $\delta^{13}C$ and δD values becoming less negative in the residue methane (Coleman et al., 1981; Hornibrook et al., 1997; Wang et al., 2016), while $\delta^{13}C$ and δD values may either increase or decrease during anaerobic oxidation of methane (AOM), depending on the reversibility of intracellular reactions (Holler et al., 2009; Liu, Harris, et al., 2023; Yoshinaga et al., 2014). In terrestrial and coastal environments, the reversibility of AOM is typically low due to the high availability of free energy, leading to less negative $\delta^{13}C$ and δD values (Liu, Harris, et al., 2023). Therefore, oxidation can cause overlapping isotopic signatures between microbial and thermogenic methane. Landfill, where high levels of AeOM activity frequently occur, exhibit varying degrees of oxidation depending on seasonal changes and landfill operations (Bakkaloglu et al., 2021; Chanton & Liptay, 2000; Spokas et al., 2021). The extent of methane oxidation determines how far the residual methane will fractionate from its original compositions (Chanton et al., 2008).

At least five different methane transport mechanisms have been identified (Bastviken et al., 2004; Johnson et al., 2022): ebullition, diffusion, the release of stored methane due to water turnover, emissions through aquatic vegetation (Sebacher et al., 1985), and ice-bubble storage flux (Walter et al., 2006). Each of these mechanisms has different temporal and spatial characteristics (DelSontro et al., 2011; Greene et al., 2014; Johnson et al., 2022; Sanches et al., 2019). For example, diffusion flux can be relatively stable at least in summer, while the release of storage methane can cause a big pulse in spring and autumn (Engle & Melack, 2000). The varying release mechanisms likely influence the isotopic signatures of the emitted methane (Walter et al., 2008).

The analysis in Section 4.1.4 reveals a seasonal pattern in the derived $\delta^{12}CH_3D_{source}$ values (Figure 8) from autumn through winter; the $\delta^{12}CH_3D$ values of methane emitted from wetlands in our study area became progressively less negative, and upon entering spring, these values shift back to more negative $\delta^{12}CH_3D$ values, with fluctuations of up to 40‰. Such a directional change is also observed in $\delta^{13}CH_4$, $\delta^{12}CH_3D$, $\Delta^{13}CH_3D$, and $\Delta^{12}CH_2D_2$ values of the selected end-members "Wetland 1" and "Wetland 2" in Section 4.1.3. Excluding the Chaneyville Rd. samples, which display significantly more negative $\delta^{12}CH_3D$ values, the remaining samples from the Patuxent River series have similar isotopic signatures to those from Jug Bay within the same season, suggesting a consistent seasonal trend across different locations within the study area.

Similar or different seasonal variations in the isotopic signals of wetland methane emissions have been observed in multiple studies. Happell et al. (1994) noted that during flooding periods, emitted methane had less negative $\delta^{13}C$ and δD, attributing to increased oxidation. Burke et al. (1988, 1992) observed a similar pattern for δD but an inverse pattern for $\delta^{13}C$ (i.e., $\delta^{13}C$ is inversely related to δD), suggesting that these opposing signals reflect differing contributions from acetotrophic and hydrogenotrophic methanogenesis pathways. Data from Sriskantharajah et al. (2012) and Fisher et al. (2017) might indicate a distinct seasonal pattern, controlled strongly by the freeze-thaw cycle in high-latitude wetlands. There are diverse factors that can contribute to seasonal variations in wetland methane emissions (France et al., 2022).
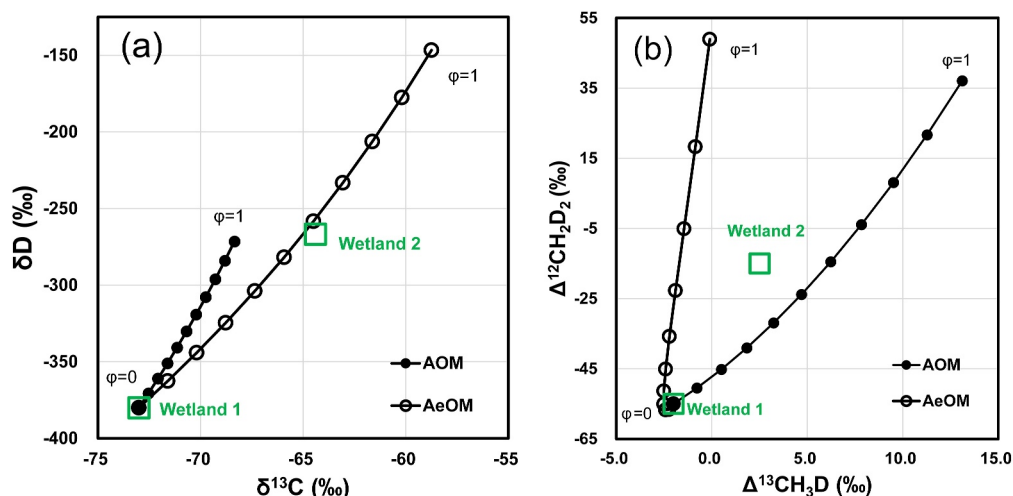
Figure 9. The (a) isotopic and (b) isotopologue fractionation trends of methane undergoing varying degrees of open-system AOM (solid circles) and AeOM (hollow circles). The initial composition is set to be Wetland 1. The fractionation factors for AeOM are adopted from Krause et al. (2022), while those for AOM are taken from Liu, Harris, et al. (2023). φ represents the fraction of methane removed through oxidation (as opposed to transport).

Unlike direct wetland sampling, the compositions we derived from air samples provide regionally integrated emission signals, which are anticipated to smooth out localized variances. Our analysis still revealed considerable variability in the derived wetland compositions, suggesting that regional controls rooted in process-based factors are governing the isotopic signals. We propose one hypothesis as an example to explain the observed variability in isotopic signals: the variability is caused by differing extents of microbial oxidation. Using the open-system models presented in Hayes (2001) and Wang et al. (2016), we performed simulations to illustrate how the isotopic signals of methane change during AeOM and AOM, starting with the initial compositions of Wetland 1. The isotopic fractionation coefficient for AeOM were taken from Krause et al. (2022), while those for AOM were derived from Liu, Harris, et al. (2023). The modeling results (Figure 9) indicate that a combination of AOM and AeOM to a certain degree can approximately replicate the composition of Wetland 2—at least in terms of the direction of isotope fractionation.

Quantitative PCR and pyrosequencing results conducted in the Jug Bay wetland area provide evidence that both aerobic and anaerobic methane-oxidizing microorganisms are present in this region (Haghnegahdar et al., 2024; Prasse et al., 2015). The water salinity and dissolved oxygen data described in Supporting Information S1 (Note S2) are not in conflict with this hypothesis. During the summer, dissolved oxygen concentrations in wetland waters are lower than in winter (Figure S3 in Supporting Information S1). There is also a slight increase in water salinity upon entering fall, (Figure S4 in Supporting Information S1), suggesting an increased availability of sulfate to act as an oxidant. Wetland environment is more conducive to microbial oxidation in winter than summer. This is consistent with our derived wetland end-member isotopic signatures, which are less negative in δ^{13}C and δD in the winter, indicating that a higher proportion of the produced methane undergoes oxidation.

However, it is important to acknowledge that variations in methanogenesis pathways and differences in substrate compositions can influence the initial methane isotopic compositions. Moreover, the isotopic fractionation coefficients of AeOM and AOM can vary within a certain range. Many combinations of these factors can be used to numerically explain the observed variability in isotopic signals. The positive relationship between δ^{13}CH$_4$ and δ^{12}CH$_3$D values (Figure 7) may suggest that a transition in methanogenesis pathways is unlikely to be the primary cause of the derived isotopic signal variations, as such transitions typically result in δ^{13}C and δD shifting in opposite directions (Burke et al., 1988, 1992). But the possibility that transitions in methanogenesis pathways have some influence on the observed isotopic signals cannot be ruled out. The specific microbial processes occurring in wetlands causing the observed isotopic signal variability should be further investigated by studies focusing on wetland methane-related microbiology.
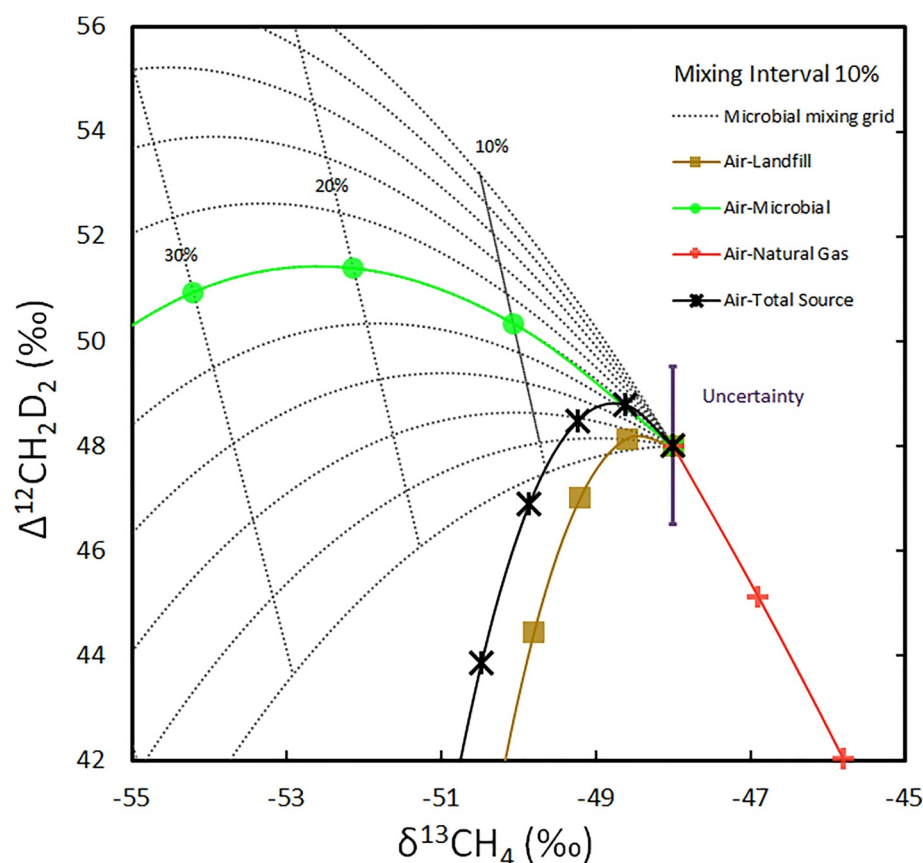
Figure 10. The zoomed in mixing curves of air with various sources, including landfill, microbial, natural gas, and total source. The landfill mixing curve is brown with square markers. The microbial curve is green with circular markers. Natural gas is red with plus signs. The total source is black with star markers. The compositions of each source can be found in Table 1. The gray mixing grid is the same as the grid in Figure 4. The mixing intervals indicated in this figure are at 10%. The typical uncertainty for $\Delta^{12}CH_2D_2$ measurements (1σ) is represented in the figure with an error bar.

4.3. Implications for Future Air Clumped Isotopologue Studies

The findings of this study present an exciting prospect: by analyzing air samples collected over emission sources, it is possible to deduce the source compositions, including clumped isotopologues. Wetland air samples appear to reveal seasonal variations in the isotopic signatures of regional wetlands (the Jug Bay). Understanding the drivers behind this variability in future studies will be essential for more precisely constraining methane emissions from wetlands on a broader scale. To achieve this, more comprehensive field surveys and air samplings are needed. The efforts should involve collecting detailed meteorological, hydrological, and environmental data, combined with isotopic and isotopologue measurements of both direct wetland samples and air samples. Furthermore, given that different wetlands respond differently across seasons, sustained monitoring of multiple wetlands with diverse ecological settings could be valuable.

Another inference from this study is that the clumped isotopologue signals of air methane are relatively insensitive to low-proportion mixing from sources, and this presents its own opportunities for information about atmospheric methane. To demonstrate this, we select four source end-members: landfill, microbial, natural gas, and total source, with their compositions listed in Table 1. The landfill composition is the Brown Station emission composition derived in Section 4.1.2. The microbial composition is a 50/50 blend of "Wetland 1" and "Wetland 2" selected in Section 4.1.3. The natural gas composition is the Panorama measurement results of the Marcellus natural gas sample (Haghnegahdar et al., 2023). The $\delta^{13}C$ and δD values of the total source follow those defined by Chung and Arnold (2021), while $\Delta^{13}CH_3D$ and $\Delta^{12}CH_2D_2$ are derived from Haghnegahdar et al. (2023). These end-members were mixed with background air (Figure 10). Although it is challenging to precisely define how low the mixing ratios are needed to not significantly affect air $\Delta^{12}CH_2D_2$ values, it appears that a 5% mix from

microbial and natural gas sources does not cause changes in air $\Delta^{12}CH_2D_2$ beyond the current 1σ measurement uncertainty. For landfill methane, this proportion is 20%, and for the total source, it reaches up to 30%. In many instances, as long as air samples are collected away from known major methane emission sources, it is highly likely that these samples will meet the "clean" criteria where the clumped isotopologue signals are not significantly disturbed by the source. Based on this working hypothesis, if we leverage the existing global greenhouse gas monitoring network (such as the NOAA GML monitoring sites), collect regional clean air samples from remote areas or upwind of cities, preferably from elevated altitudes, and measure their methane clumped isotopologue signatures, the observed spatial and/or temporal variations in $\Delta^{12}CH_2D_2$ values (if they exist) could be attributed solely to fluctuations in sink reactions. These variations could be due to spatial and temporal unevenness in OH concentrations (Anderson et al., 2021; Lu & Khalil, 1991), or fluctuations in the ratio of OH to Cl concentrations (Gromov et al., 2018; Platt et al., 2004; Solomon et al., 1997), such as during tropospheric intrusion events (Greenslade et al., 2017; Liang & Mahata, 2015). If we can obtain a sufficient number of high-precision measurements of methane clumped isotopologues in clean air, it may enable a more detailed investigation of atmospheric methane sink reactions from an isotopic perspective.

5. Summary

In this study, we investigated regional methane emissions, collecting air samples above wetlands and within landfill plumes to analyze the carbon and hydrogen isotope ratios, and clumped isotopologue compositions of methane. Employing a three-end-member (background air, landfill, and wetland) mixing framework, we established the compositions of the background air and utilized the Keeling plot method to derive the compositions of landfill and wetland methane. Furthermore, we developed a mathematical approach leveraging methane clumped isotopologue data to estimate the bulk isotope compositions of wetland methane independently of concentration data. This method overcomes the amplification of uncertainties associated with concentration data, which is a major limitation of the Keeling plot method, resulting in lower uncertainties in derived wetland emission isotopic signatures.

Our findings reveal significant seasonal variations in the isotopic and isotopologue signatures of regionally integrated methane emissions, which we attribute to different oxidation levels, with a trend toward greater oxidation signatures in winter. This research advances our understanding of regional wetland methane dynamics and contributes to refining the global methane budget. Our results advocate for systematic isotopic and isotopologue monitoring of methane emissions from wetlands, coupled with fieldwork, to uncover seasonal emission patterns and gain more insights into their driving processes.

Conflict of Interest

The authors declare no conflicts of interest relevant to this study.

Data Availability Statement

All measured data in this study are included in the Supporting Information S1 (Table S1, Table S2, Table S4, Figure S3, and Figure S4). Some are also plotted in the main text (Figures 1–6). The Excel tables used for this work, the code for generating some of the figures in this work, and the raw data tables from Panorama measurements are included in the Data Set S1 and are also available at the Digital Repository for the University of Maryland (DRUM) via http://hdl.handle.net/1903/33660 with free access (Sun, Magen, et al., 2025).

References

Alperin, M. J., Reeburgh, W. S., & Whiticar, M. J. (1988). Carbon and hydrogen isotope fractionation resulting from anaerobic methane oxidation. *Global Biogeochemical Cycles*, *2*(3), 279–288. https://doi.org/10.1029/GB002i003p00279

Anderson, D. C., Duncan, B. N., Fiore, A. M., Baublitz, C. B., Follette-Cook, M. B., Nicely, J. M., & Wolfe, G. M. (2021). Spatial and temporal variability in the hydroxyl (OH) radical: Understanding the role of large-scale climate features and their influence on OH through its dynamical and photochemical drivers. *Atmospheric Chemistry and Physics*, *21*(8), 6481–6508. https://doi.org/10.5194/acp-21-6481-2021

Bakkaloglu, S., Lowry, D., Fisher, R. E., France, J. L., Brunner, D., Chen, H., & Nisbet, E. G. (2021). Quantification of methane emissions from UK biogas plants. *Waste Management*, *124*, 82–93. https://doi.org/10.1016/j.wasman.2021.01.011

Bakkaloglu, S., Lowry, D., Fisher, R. E., Menoud, M., Lanoisellé, M., Chen, H., et al. (2022). Stable isotopic signatures of methane from waste sources through atmospheric measurements. *Atmospheric Environment*, *276*, 119021. https://doi.org/10.1016/j.atmosenv.2022.119021

Bakwin, P. S., Tans, P. P., White, J. W. C., & Andres, R. J. (1998). Determination of the isotopic (^{13}C/^{12}C) discrimination by terrestrial biology from a global network of observations. *Global Biogeochemical Cycles*, *12*(3), 555–562. https://doi.org/10.1029/98GB02265

Bastviken, D., Cole, J., Pace, M., & Tranvik, L. (2004). Methane emissions from lakes: Dependence of lake characteristics, two regional assessments, and a global estimate. *Global Biogeochemical Cycles*, *18*(4), GB4009. https://doi.org/10.1029/2004GB002238

Burke, R. A., Barber, T. R., & Sackett, W. M. (1992). Seasonal variations of stable hydrogen and carbon isotope ratios of methane in subtropical freshwater sediments. *Global Biogeochemical Cycles*, *6*(2), 125–138. https://doi.org/10.1029/92GB00155

Burke, R. A., Martens, C. S., & Sackett, W. M. (1988). Seasonal variations of D/H and $^{13}C/^{12}C$ ratios of microbial methane in surface sediments. *Nature*, *332*(6167), 829–831. https://doi.org/10.1038/332829a0

Cao, X., Bao, H., & Peng, Y. (2019). A kinetic model for isotopologue signatures of methane generated by biotic and abiotic CO_2 methanation. *Geochimica et Cosmochimica Acta*, *249*, 59–75. https://doi.org/10.1016/j.gca.2019.01.021

Chanton, J., & Liptay, K. (2000). Seasonal variation in methane oxidation in a landfill cover soil as determined by an in situ stable isotope technique. *Global Biogeochemical Cycles*, *14*(1), 51–60. https://doi.org/10.1029/1999GB900087

Chanton, J. P., Powelson, D. K., Abichou, T., & Hater, G. (2008). Improved field methods to quantify methane oxidation in landfill cover materials using stable carbon isotopes. *Environmental Science & Technology*, *42*(3), 665–670. https://doi.org/10.1021/es0710757

Chesapeake Bay Program. (2019). Retrieved from https://www.chesapeakebay.net/what/maps/chesapeake-bay-mean-surface-salinity-1985-2018

Chung, E., & Arnold, T. (2021). Potential of clumped isotopes in constraining the global atmospheric methane budget. *Global Biogeochemical Cycles*, *35*(10), e2020GB006883. https://doi.org/10.1029/2020GB006883

Coleman, D. D., Risatti, J. B., & Schöll, M. (1981). Fractionation of carbon and hydrogen isotopes by methane-oxidizing bacteria. *Geochimica et Cosmochimica Acta*, *45*(7), 1033–1037. https://doi.org/10.1016/0016-7037(81)90129-0

Conrad, R. (2005). Quantification of methanogenic pathways using stable carbon isotopic signatures: A review and a proposal. *Organic Geochemistry*, *36*(5), 739–752. https://doi.org/10.1016/j.orggeochem.2004.09.006

Coplen, T. B. (1994). Reporting of stable hydrogen, carbon, and oxygen isotopic abundances (Technical Report). *Pure and Applied Chemistry*, *66*(2), 273–276. https://doi.org/10.1351/pac199466020273

DelSontro, T., Kunz, M. J., Kempter, T., Wüest, A., Wehrli, B., & Senn, D. B. (2011). Spatial heterogeneity of methane ebullition in a large tropical reservoir. *Environmental Science & Technology*, *45*(23), 9866–9873. https://doi.org/10.1021/es2005545

DelSontro, T., McGinnis, D. F., Wehrli, B., & Ostrovsky, I. (2015). Size does matter: Importance of large bubbles and small-scale hot spots for methane transport. *Environmental Science & Technology*, *49*(3), 1268–1276. https://doi.org/10.1021/es5054286

Douglas, P., Stolper, D., Smith, D., Anthony, K. W., Paull, C., Dallimore, S., et al. (2016). Diverse origins of Arctic and Subarctic methane point source emissions identified with multiply-substituted isotopologues. *Geochimica et Cosmochimica Acta*, *188*, 163–188. https://doi.org/10.1016/j.gca.2016.05.031

Douglas, P. M. J., Gonzalez Moguel, R., Walter Anthony, K. M., Wik, M., Crill, P. M., Dawson, K. S., et al. (2020). Clumped isotopes link older carbon substrates with slower rates of methanogenesis in northern lakes. *Geophysical Research Letters*, *47*(6), e2019GL086756. https://doi.org/10.1029/2019gl086756

Eiler, J. M., & Schauble, E. (2004). $^{18}O^{13}C^{16}O$ in Earth's atmosphere. *Geochimica et Cosmochimica Acta*, *68*(23), 4767–4777. https://doi.org/10.1016/j.gca.2004.05.035

Engle, D., & Melack, J. M. (2000). Methane emissions from an Amazon floodplain lake: Enhanced release during episodic mixing and during falling water. *Biogeochemistry*, *51*(1), 71–90. https://doi.org/10.1023/A:1006389124823

Environmental Integrity Project. (2021). Greenhouse gases from Maryland's landfills underestimated and under regulated [Dataset]. Retrieved from https://environmentalintegrity.org/wp-content/uploads/2021/06/MD-Landfill-Methane-Report-6.9.2021-unembargoed_with-Attachments.pdf

Fisher, R. E., France, J. L., Lowry, D., Lanoisellé, M., Brownlow, R., Pyle, J. A., et al. (2017). Measurement of the ^{13}C isotopic signature of methane emissions from northern European wetlands. *Global Biogeochemical Cycles*, *31*(3), 605–623. https://doi.org/10.1002/2016GB005504

Fisher, R. E., Sriskantharajah, S., Lowry, D., Lanoisellé, M., Fowler, C., James, R., et al. (2011). Arctic methane sources: Isotopic evidence for atmospheric inputs. *Geophysical Research Letters*, *38*(21). https://doi.org/10.1029/2011GL049319

France, J. L., Lunt, M. F., Andrade, M., Moreno, I., Ganesan, A. L., Lachlan-Cope, T., et al. (2022). Very large fluxes of methane measured above Bolivian seasonal wetlands. *Proceedings of the National Academy of Sciences of the United States of America*, *119*(32), e2206345119. https://doi.org/10.1073/pnas.2206345119

Ganesan, A., Stell, A., Gedney, N., Comyn-Platt, E., Hayman, G., Rigby, M., et al. (2018). Spatially resolved isotopic source signatures of wetland methane emissions. *Geophysical Research Letters*, *45*(8), 3737–3745. https://doi.org/10.1002/2018GL077536

Giunta, T., Young, E. D., Labidi, J., Sansjofre, P., Jézéquel, D., Donval, J.-P., et al. (2022). Extreme methane clumped isotopologue bio-signatures of aerobic and anaerobic methanotrophy: Insights from the Lake Pavin and the Black Sea sediments. *Geochimica et Cosmochimica Acta*, *338*, 34–53. https://doi.org/10.1016/j.gca.2022.09.034

Giunta, T., Young, E. D., Warr, O., Kohl, I., Ash, J. L., Martini, A., et al. (2019). Methane sources and sinks in continental sedimentary systems: New insights from paired clumped isotopologues $^{13}CH_3D$ and $^{12}CH_2D_2$. *Geochimica et Cosmochimica Acta*, *245*, 327–351. https://doi.org/10.1016/j.gca.2018.10.030

Greene, S., Walter Anthony, K. M., Archer, D., Sepulveda-Jauregui, A., & Martinez-Cruz, K. (2014). Modeling the impediment of methane ebullition bubbles by seasonal lake ice. *Biogeosciences*, *11*(23), 6791–6811. https://doi.org/10.5194/bg-11-6791-2014

Greenslade, J. W., Alexander, S. P., Schofield, R., Fisher, J. A., & Klekociuk, A. K. (2017). Stratospheric ozone intrusion events and their impacts on tropospheric ozone in the Southern Hemisphere. *Atmospheric Chemistry and Physics*, *17*(17), 10269–10290. https://doi.org/10.5194/acp-17-10269-2017

Gromov, S., Brenninkmeijer, C. A., & Jöckel, P. (2018). A very limited role of tropospheric chlorine as a sink of the greenhouse gas methane. *Atmospheric Chemistry and Physics*, *18*(13), 9831–9843. https://doi.org/10.5194/acp-18-9831-2018

Gropp, J., Iron, M. A., & Halevy, I. (2021). Theoretical estimates of equilibrium carbon and hydrogen isotope effects in microbial methane production and anaerobic oxidation of methane. *Geochimica et Cosmochimica Acta*, *295*, 237–264. https://doi.org/10.1016/j.gca.2020.10.018

Gropp, J., Jin, Q., & Halevy, I. (2022). Controls on the isotopic composition of microbial methane. *Science Advances*, *8*(14), eabm5713. https://doi.org/10.1126/sciadv.abm5713

Gruen, D. S., Wang, D. T., Könneke, M., Topçuoğlu, B. D., Stewart, L. C., Goldhammer, T., et al. (2018). Experimental investigation on the controls of clumped isotopologue and hydrogen isotope ratios in microbial methane. *Geochimica et Cosmochimica Acta*, *237*, 339–356. https://doi.org/10.1016/j.gca.2018.06.029

Haghnegahdar, M. (2018). Theoretical study of tellurium isotope fractionations in ore-forming systems, and studies of doubly substituted isotopologues of methane (Publication Number Haghnegahdar_ucla_0031D_17475) UCLA]. Retrieved from https://escholarship.org/uc/item/7bd5c85d

Haghnegahdar, M. A., Hultquist, N., Hamovit, N. D., Yarwood, S. A., Bouyon, A., Kaufman, A. J., et al. (2024). A better understanding of atmospheric methane sources using $^{13}CH3D$ and $^{12}CH_2D_2$ clumped isotopes. *Journal of Geophysical Research: Biogeosciences*, *129*(11), e2024JG008172. https://doi.org/10.1029/2024JG008172

Haghnegahdar, M. A., Sun, J., Hultquist, N., Hamovit, N. D., Kitchen, N., Eiler, J., et al. (2023). Tracing sources of atmospheric methane using clumped isotopes. *Proceedings of the National Academy of Sciences of the United States of America*, *120*(47), e2305574120. https://doi.org/10.1073/pnas.2305574120

Happell, J. D., Chanton, J. P., & Showers, W. S. (1994). The influence of methane oxidation on the stable isotopic composition of methane emitted from Florida swamp forests. *Geochimica et Cosmochimica Acta*, *58*(20), 4377–4388. https://doi.org/10.1016/0016-7037(94)90341-7

Hayes, J. M. (2001). Fractionation of carbon and hydrogen isotopes in biosynthetic processes*. *Reviews in Mineralogy and Geochemistry*, *43*(1), 225–277. https://doi.org/10.2138/gsrmg.43.1.225

Holler, T., Wegener, G., Knittel, K., Boetius, A., Brunner, B., Kuypers, M. M. M., & Widdel, F. (2009). Substantial $^{13}C/^{12}C$ and D/H fractionation during anaerobic oxidation of methane by marine consortia enriched in vitro. *Environmental Microbiology Reports*, *1*(5), 370–376. https://doi.org/10.1111/j.1758-2229.2009.00074.x

Hornibrook, E. R. C., Longstaffe, F. J., & Fyfe, W. S. (1997). Spatial distribution of microbial methane production pathways in temperate zone wetland soils: Stable carbon and hydrogen isotope evidence. *Geochimica et Cosmochimica Acta*, *61*(4), 745–753. https://doi.org/10.1016/S0016-7037(96)00368-7

Johnson, M. S., Matthews, E., Du, J., Genovese, V., & Bastviken, D. (2022). Methane emission from global lakes: New spatiotemporal data and observation-driven modeling of methane dynamics indicates lower emissions. *Journal of Geophysical Research: Biogeosciences*, *127*(7), e2022JG006793. https://doi.org/10.1029/2022JG006793

Karion, A., Callahan, W., Stock, M., Prinzivalli, S., Verhulst, K. R., Kim, J., et al. (2020). Greenhouse gas observations from the Northeast Corridor tower network. *Earth System Science Data*, *12*(1), 699–717. https://doi.org/10.5194/essd-12-699-2020

Keeling, C. D. (1958). The concentration and isotopic abundances of atmospheric carbon dioxide in rural areas. *Geochimica et Cosmochimica Acta*, *13*(4), 322–334. https://doi.org/10.1016/0016-7037(58)90033-4

Krause, S. J. E., Liu, J., Young, E. D., & Treude, T. (2022). $\Delta^{13}CH_3D$ and $\Delta^{12}CH_2D_2$ signatures of methane aerobically oxidized by Methylosinus trichosporium with implications for deciphering the provenance of methane gases. *Earth and Planetary Science Letters*, *593*, 117681. https://doi.org/10.1016/j.epsl.2022.117681

Lan, X., Thoning, K. W., & Dlugokencky, E. J. (2025). Trends in globally-averaged CH_4, N_2O, and SF_6 determined from NOAA Global Monitoring Laboratory measurements. Version 2025-03. https://doi.org/10.15138/P8XG-AA10

Langenegger, T., Vachon, D., Donis, D., & McGinnis, D. F. (2019). What the bubble knows: Lake Methane dynamics revealed by sediment gas bubble composition. *Limnology & Oceanography*, *64*(4), 1526–1544. https://doi.org/10.1002/lno.11133

Li, J., Ash, J. L., Cobban, A., Kubik, B. C., Rizzo, G., Thompson, M., et al. (2024). The clumped isotope signatures of multiple methanogenesis metabolisms. bioRxiv, 2024.2012.2018.629299. https://doi.org/10.1101/2024.12.18.629299

Li, J., Chiu, B. K., Piasecki, A. M., Feng, X., Landis, J. D., Marcum, S., et al. (2024). The evolution of multiply substituted isotopologues of methane during microbial aerobic oxidation. *Geochimica et Cosmochimica Acta*, *381*, 223–238. https://doi.org/10.1016/j.gca.2024.06.032

Liang, M.-C., & Mahata, S. (2015). Oxygen anomaly in near surface carbon dioxide reveals deep stratospheric intrusion. *Scientific Reports*, *5*(1), 11352. https://doi.org/10.1038/srep11352

Liu, J. (2024). *The biogeochemistry of methane cycling and its clumped isotope effects*. University of California, ProQuest Dissertations & Theses Global. Retrieved from https://escholarship.org/uc/item/62d7r8rs

Liu, J., Harris, R. L., Ash, J. L., Ferry, J. G., Krause, S. J. E., Labidi, J., et al. (2023). Reversibility controls on extreme methane clumped isotope signatures from anaerobic oxidation of methane. *Geochimica et Cosmochimica Acta*, *348*, 165–186. https://doi.org/10.1016/j.gca.2023.02.022

Liu, J., Treude, T., Abbasov, O. R., Baloglanov, E. E., Aliyev, A. A., Harris, C. M., et al. (2023). Clumped isotope evidence for microbial alteration of thermogenic methane in terrestrial mud volcanoes. *Geology*, *52*(1), 22–26. https://doi.org/10.1130/G51667.1

Lu, Y., & Khalil, M. A. K. (1991). Tropospheric OH: Model calculations of spatial, temporal, and secular variations. *Chemosphere*, *23*(3), 397–444. https://doi.org/10.1016/0045-6535(91)90194-I

Luxem Katja, E., Leavitt William, D., & Zhang, X. (2020). Large hydrogen isotope fractionation distinguishes nitrogenase-derived methane from other methane sources. *Applied and Environmental Microbiology*, *86*(19). https://doi.org/10.1128/AEM.00849-20

Milkov, A. V., & Etiope, G. (2018). Revised genetic diagrams for natural gases based on a global dataset of >20,000 samples. *Organic Geochemistry*, *125*, 109–120. https://doi.org/10.1016/j.orggeochem.2018.09.002

NOAA National Estuarine Research Reserve System (NERRS). (2025). System-wide Monitoring Program. Data accessed from the NOAA NERRS Centralized Data Management Office. Retrieved from http://www.nerrsdata.org

Ono, S., Rhim, J. H., Gruen, D. S., Taubner, H., Kölling, M., & Wegener, G. (2021). Clumped isotopologue fractionation by microbial cultures performing the anaerobic oxidation of methane. *Geochimica et Cosmochimica Acta*, *293*, 70–85. https://doi.org/10.1016/j.gca.2020.10.015

Ono, S., Rhim, J. H., & Ryberg, E. C. (2022). Rate limits and isotopologue fractionations for microbial methanogenesis examined with combined pathway protein cost and isotopologue flow network models. *Geochimica et Cosmochimica Acta*, *325*, 296–315. https://doi.org/10.1016/j.gca.2022.03.017

Platt, U., Allan, W., & Lowe, D. (2004). Hemispheric average Cl atom concentration from $^{13}C/^{12}C$ ratios in atmospheric methane. *Atmospheric Chemistry and Physics*, *4*(9/10), 2393–2399. https://doi.org/10.5194/acp-4-2393-2004

Prasse, C. E., Baldwin, A. H., & Yarwood, S. A. (2015). Site history and edaphic features override the influence of plant species on microbial communities in restored tidal freshwater wetlands. *Applied and Environmental Microbiology*, *81*(10), 3482–3491. https://doi.org/10.1128/AEM.00038-15

Ren, X., Hall, D. L., Vinciguerra, T., Benish, S. E., Stratton, P. R., Ahn, D., et al. (2019). Methane emissions from the Marcellus Shale in Southwestern Pennsylvania and northern West Virginia based on airborne measurements. *Journal of Geophysical Research: Atmospheres*, *124*(3), 1862–1878. https://doi.org/10.1029/2018JD029690

Ren, X., Salmon, O. E., Hansford, J. R., Ahn, D., Hall, D., Benish, S. E., et al. (2018). Methane emissions from the baltimore-Washington area based on airborne observations: Comparison to emissions inventories. *Journal of Geophysical Research: Atmospheres*, *123*(16), 8869–8882. https://doi.org/10.1029/2018JD028851

Rhim, J. H., & Ono, S. (2022). Combined carbon, hydrogen, and clumped isotope fractionations reveal differential reversibility of hydrogenotrophic methanogenesis in laboratory cultures. *Geochimica et Cosmochimica Acta*, *335*, 383–399. https://doi.org/10.1016/j.gca.2022.07.027

Sanches, L. F., Guenet, B., Marinho, C. C., Barros, N., & de Assis Esteves, F. (2019). Global regulation of methane emission from natural lakes. *Scientific Reports*, *9*(1), 255. https://doi.org/10.1038/s41598-018-36519-5

Sebacher, D. I., Harriss, R. C., & Bartlett, K. B. (1985). Methane emissions to the atmosphere through aquatic plants. *Journal of Environmental Quality*, *14*(1), 40–46. https://doi.org/10.2134/jeq1985.00472425001400010008x

Solomon, S., Borrmann, S., Garcia, R. R., Portmann, R., Thomason, L., Poole, L. R., et al. (1997). Heterogeneous chlorine chemistry in the tropopause region. *Journal of Geophysical Research*, *102*(D17), 21411–21429. https://doi.org/10.1029/97JD01525

Spokas, K., Bogner, J., & Corcoran, M. (2021). Modeling landfill CH_4 emissions: CALMIM international field validation, using CALMIM to simulate management strategies, current and future climate scenarios. *Elementa: Science of the Anthropocene*, *9*(1), 00050. https://doi.org/10.1525/elementa.2020.00050

Sriskantharajah, S., Fisher, R., Lowry, D., Aalto, T., Hatakka, J., Aurela, M., et al. (2012). Stable carbon isotope signatures of methane from a Finnish subarctic wetland. *Tellus B: Chemical and Physical Meteorology*, *64*(1), 18818. https://doi.org/10.3402/tellusb.v64i0.18818

Stolper, D. A., Lawson, M., Davis, C. L., Ferreira, A. A., Neto, E. V. S., Ellis, G. S., et al. (2014). Formation temperatures of thermogenic and biogenic methane. *Science*, *344*(6191), 1500–1503. https://doi.org/10.1126/science.1254509

Stolper, D. A., Martini, A. M., Clog, M., Douglas, P. M., Shusta, S. S., Valentine, D. L., et al. (2015). Distinguishing and understanding thermogenic and biogenic sources of methane using multiply substituted isotopologues. *Geochimica et Cosmochimica Acta*, *161*, 219–247. https://doi.org/10.1016/j.gca.2015.04.015

Stolper, D. A., Sessions, A. L., Ferreira, A. A., Santos Neto, E. V., Schimmelmann, A., Shusta, S. S., et al. (2014). Combined 13C–D and D–D clumping in methane: Methods and preliminary results. *Geochimica et Cosmochimica Acta*, *126*, 169–191. https://doi.org/10.1016/j.gca.2013.10.045

Sun, J., Haghnegahdar, M. A., Fernandez, J. M., Magen, C., & Farquhar, J. (2025). Controls on concentrations and clumped isotopologues of vehicle exhaust methane. *PLoS One*, *20*(2), e0315304. https://doi.org/10.1371/journal.pone.0315304

Sun, J., Magen, C., Haghnegahdar, M. A., Liu, J., Fernandez, J. M., & Farquhar, J. (2025). Dataset for constraining wetland and landfill methane emission signatures through atmospheric methane clumped isotopologue measurements (version 1) [Dataset]. *Digital Repository for the University of Maryland*. http://hdl.handle.net/1903/33660

Taenzer, L., Labidi, J., Masterson, A. L., Feng, X., Rumble, D., Young, E. D., & Leavitt, W. D. (2020). Low $\Delta^{12}CH_2D_2$ values in microbialgenic methane result from combinatorial isotope effects. *Geochimica et Cosmochimica Acta*, *285*, 225–236. https://doi.org/10.1016/j.gca.2020.06.026

Walter, K. M., Chanton, J. P., Chapin Iii, F. S., Schuur, E. A. G., & Zimov, S. A. (2008). Methane production and bubble emissions from arctic lakes: Isotopic implications for source pathways and ages. *Journal of Geophysical Research*, *113*(G3). https://doi.org/10.1029/2007JG000569

Walter, K. M., Zimov, S. A., Chanton, J. P., Verbyla, D., & Chapin, F. S. (2006). Methane bubbling from Siberian thaw lakes as a positive feedback to climate warming. *Nature*, *443*(7107), 71–75. https://doi.org/10.1038/nature05040

Wang, D. T., Gruen, D. S., Lollar, B. S., Hinrichs, K.-U., Stewart, L. C., Holden, J. F., et al. (2015). Nonequilibrium clumped isotope signals in microbial methane. *Science*, *348*(6233), 428–431. https://doi.org/10.1126/science.aaa4326

Wang, D. T., Welander, P. V., & Ono, S. (2016). Fractionation of the methane isotopologues $^{13}CH_4$, $^{12}CH_3D$, and $^{13}CH_3D$ during aerobic oxidation of methane by Methylococcus capsulatus (Bath). *Geochimica et Cosmochimica Acta*, *192*, 186–202. https://doi.org/10.1016/j.gca.2016.07.031

Whiticar, M. J. (1999). Carbon and hydrogen isotope systematics of bacterial formation and oxidation of methane. *Chemical Geology*, *161*(1–3), 291–314. https://doi.org/10.1016/S0009-2541(99)00092-3

Whiticar, M. J., Faber, E., & Schöll, M. (1986). Biogenic methane formation in marine and freshwater environments: CO_2 reduction vs. acetate fermentation—Isotope evidence. *Geochimica et Cosmochimica Acta*, *50*(5), 693–709. https://doi.org/10.1016/0016-7037(86)90346-7

Wik, M., Thornton, B. F., Bastviken, D., Uhlbäck, J., & Crill, P. M. (2016). Biased sampling of methane release from northern lakes: A problem for extrapolation. *Geophysical Research Letters*, *43*(3), 1256–1262. https://doi.org/10.1002/2015GL066501

Yoshinaga, M. Y., Holler, T., Goldhammer, T., Wegener, G., Pohlman, J. W., Brunner, B., et al. (2014). Carbon isotope equilibration during sulphate-limited anaerobic oxidation of methane. *Nature Geoscience*, *7*(3), 190–194. https://doi.org/10.1038/ngeo2069

Young, E. D. (2019). A two-dimensional perspective on CH_4 isotope clumping: Distinguishing process from source. In I. D. BN Orcutt & R. Dasgupta (Eds.), *Deep Carbon: Past to Present* (pp. 388–414). Cambridge University Press. https://doi.org/10.1017/9781108677950.013

Young, E. D., Kohl, I. E., Lollar, B. S., Etiope, G., Rumble, D., Li, S., et al. (2017). The relative abundances of resolved $^{12}CH_2D_2$ and $^{13}CH_3D$ and mechanisms controlling isotopic bond ordering in abiotic and biotic methane gases. *Geochimica et Cosmochimica Acta*, *203*, 235–264. https://doi.org/10.1016/j.gca.2016.12.041

Young, E. D., Rumble, D., Freedman, P., & Mills, M. (2016). A large-radius high-mass-resolution multiple-collector isotope ratio mass spectrometer for analysis of rare isotopologues of O_2, N_2, CH_4 and other gases. *International Journal of Mass Spectrometry*, *401*, 1–10. https://doi.org/10.1016/j.ijms.2016.01.006